IS-T 1894

Magnetocaloric Effect of Gd*4*(Bi*x*Sb*1-x*)*3* Alloy Series

by

Niu, Xuejun

MS Thesis submitted to Iowa State University

Ames Laboratory, U.S. DOE
Iowa State University
Ames, Iowa 50011

Date 1999

PREPARED FOR THE U.S. DEPARTMENT OF ENERGY
UNDER CONTRACT NO. W-7405-Eng-82.

DISCLAIMER

This report has been reproduced directly from the best available copy.

AVAILABILITY:

To DOE and DOE contractors: Office of Scientific and Technical Information
P.O. Box 62
Oak Ridge, TN 37831

prices available from: (615) 576-8401
FTS: 626-8401

To the public: National Technical Information Service
U.S. Department of Commerce
5285 Port Royal Road
Springfield, VA 22161

DISCLAIMER

Portions of this document may be illegible in electronic image products. Images are produced from the best available original document.

TABLE OF CONTENTS

1. INTRODUCTION 1

1.1 General 1

1.2 Magnetic refrigeration and materials 8

1.3 Rationale 10

2. EXPERIMENTAL PROCEDURES 12

2.1 Sample preparation 12

2.2 X-ray measurements 13

2.3 Magnetic measurements 14

2.4 Heat capacity measurements 16

3. RESULTS AND DISCUSSION 17

3.1 Crystal structure and metallography 17

3.2 Magnetic measurements 19

3.2.1 DC magnetic susceptibility 19

3.2.2 AC magnetic susceptibility 21

3.2.3 Magnetization measurements 25

3.3 Heat capacity measurements 31

4. CONCLUSIONS 46

REFERENCES 47

ACKNOWLEDGEMENTS 49

1. INTRODUCTION

1.1 General

Magnetocaloric effect (MCE), or adiabatic temperature change, was originally discovered in iron by Warburg late in the 19th century [1]. It is the response of a magnetic material to a changing field that is evident as a change in its temperature.

The MCE is intrinsic to all magnetic materials. It is due to the coupling of the magnetic sublattice with the magnetic field, which changes the magnetic part of the total entropy of the material. For a simple ferromagnetic material near its Curie temperature, when a magnetic field is applied, the spins tend to align parallel to the magnetic field. This lowers the magnetic entropy. To compensate for the loss in the magnetic entropy in an adiabatic (isentropic) process the temperature of the material increases. When the magnetic field is turned off the spins tend to become random. This increases the magnetic entropy and the material cools.

The thermodynamics of the MCE in a ferromagnet near its Curie temperature is illustrated schematically in Figure 1.1. At constant pressure the total entropy of a magnetic material, S(T,H), which is a function of both the magnetic field strength H and the absolute temperature T, is the combined total of the magnetic entropy S_M, the lattice entropy S_{Lat}, and the electronic entropy S_{El} contributions:

$$S(T,H) = S_M(T,H) + S_{Lat}(T) + S_{El}(T) \qquad (1.1)$$

Since the change of lattice entropy S_{Lat} and electronic entropy S_{El} with magnetic field are negligible compared with magnetic entropy, only magnetic entropy is of interest here.

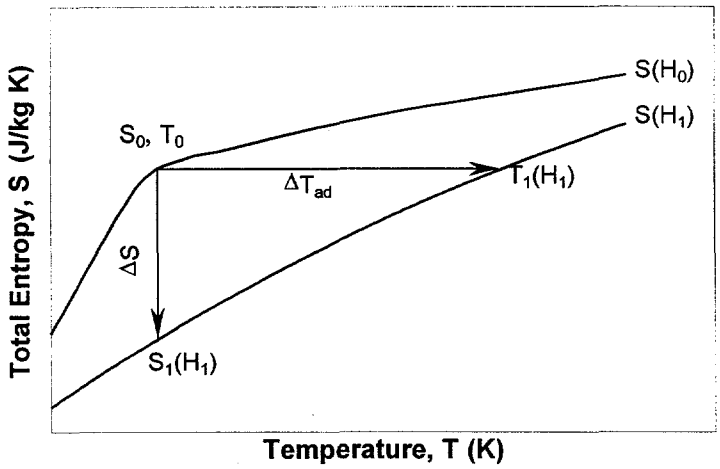

Figure 1.1 The S-T diagram schematically illustrating the existence of MCE

Figure 1.1 shows the total entropy for a ferromagnetic material in two constant fields, H_0 which is usually taken to be zero in most applications, and H_1 which is a non-zero magnetic field. When the magnetic field is applied adiabatically (i.e. when the total entropy of the system remains constant during the magnetic field change) in a reversible process, the magnetocaloric effect expressed as the adiabatic temperature rise, ΔT_{ad}, can be visualized as the isentropic difference between the corresponding S(T, H) functions as shown in Figure 1.1 by the horizontal arrow. The MCE can also be expressed by means of the isothermal magnetic entropy change, ΔS_M, when the magnetic field is applied isothermally. In the latter case it is equal to the isothermal difference between the corresponding S(T,H) functions as shown in Figure 1.1 by the vertical arrow. Therefore ΔT_{ad} and ΔS_M represent the two quantitative characteristics of the magnetocaloric effect, and it is easy to see that both ΔT_{ad} and ΔS_M are functions of the initial temperature, T_0, before the magnetic field is altered, and the magnetic field change, ΔH.

There are some substances which exhibit a negative MCE, i.e. the sample cools when a magnetic field is applied to the material and warms when it is removed. This can be easily explained by Figure 1.1. If $S(T, H_1)$ is higher than $S(T, H_0)$, raising the magnetic field will decrease the magnetic order (i.e. reduces magnetic entropy). Thus ΔT_{ad} is negative and the magnetic material cools off, while ΔS_M is positive. The signs of ΔT_{ad} and ΔS_M are correspondingly reversed when the magnetic field is reduced. Generally this occurs when one of the magnetic phases is an antiferromagnet. Also materials with unusual crystalline electric field levels have been reported to exhibit a negative MCE.

The ΔT_{ad} and ΔS_M are correlated with the magnetization, M, the magnetic field strength, the heat capacity at constant pressure, C, and the absolute temperature by one of the fundamental Maxwell's eqautions [2]

$$\left(\frac{\partial S(T,H)}{\partial H}\right)_T = \left(\frac{\partial M(T,H)}{\partial T}\right)_H \tag{1.2}$$

For isothermal-isobaric process, integrating the above equation gives

$$\Delta S_M(T,\Delta H) = \int_{H_1}^{H_2}\left(\frac{\partial M(T,H)}{\partial T}\right)_H dH \tag{1.3}$$

Considering the total entropy of the system S(T, H, p), its total differential can be written as:

$$dS = \left(\frac{\partial S}{\partial T}\right)_{H,p} dT + \left(\frac{\partial S}{\partial H}\right)_{T,p} dH + \left(\frac{\partial S}{\partial p}\right)_{T,H} dp, \tag{1.4}$$

where p is the pressure. For an adiabatic-isobaric process, the left hand side and the third term of equation (1.4) are both 0. Combining the Maxwell equation (1.2)

and considering $C(T,H) = T\left(\frac{\partial S}{\partial T}\right)_p$, the infinitesimal adiabatic temperature rise can be expressed by

$$dT = -\left(\frac{T}{C(T,H)}\right)_H \left(\frac{\partial M(T,H)}{\partial T}\right)_H dH \tag{1.5}$$

Integrating the above equations we have the value of the adiabatic temperature change

$$\Delta T_{ad} = -\int_{H_1}^{H_2} \left(\frac{T}{C(T,H)}\right)_H \left(\frac{\partial M(T,H)}{\partial T}\right)_H dH \tag{1.6}$$

All the above equations are obtained using the general principles of thermodynamics and can be used to describe the magnetocaloric effect on a macroscopic scale. On a micro-scopic scale a simple model can be derived in the framework of the MFA (mean field approximation) using statistical and quantum mechanical theory.

In this model the magnetic moment is given by [3]

$$M = NM_J B_J\left(\frac{M_J H}{k_B T}\right) \tag{1.7}$$

where N is the number of atoms in the system, $M_J = g_J \mu_B J$ (J is the total angular momentum quantum number, μ_B is the Bohr magneton, and g_J is the gyromagnetic ratio), and $B_J\left(\frac{M_J H}{k_B T}\right)$ is the Brillouin function. For $k_B T >> M_J H$, which is usually realized in an experiment, the above equation leads to the Curie law:

$$M = \frac{C}{T} H \tag{1.8a}$$

where $C = N\mu_B{}^2 g_J{}^2 J(J+1)/3k_B$ is the Curie constant.

In MFA the magnetization equation (1.8a) in the paramagnetic region takes the form of the Curie-Weiss law [3]:

$$M = \frac{CH}{T - T_C} \tag{1.8b}$$

where T_C is the Curie temperature:

$$T_C = \frac{N M_{eff}^{\ 2} \alpha}{3k_B} \tag{1.9}$$

$M_{eff} = g_J (J(J+1))^{\frac{1}{2}} \mu_B$ is the effective magnetic moment of an atom, and α is the mean field constant.

The magnetic entropy, S_M, which can be changed by variation of the magnetic field, temperature and other thermodynamic parameters, is an important characteristic of a magnetic material. S_M and ΔS_M are closely related with the MCE values and the magnetic contribution to the heat capacity. Using the Maxwell equation and the free energy expression from statistical theory, one can obtain [4]

$$S_M(T,H) = Nk_B \left[\ln \frac{\sinh\left(\frac{2J+1}{2J} x\right)}{\sinh\left(\frac{x}{2J}\right)} - x B_J(x) \right] \tag{1.10}$$

where $x = \frac{M_J H}{k_B T}$. For x << 1, which is generally satisfied under normal experimental condition, the above equation can be simplified for a paramagnet as [5]

$$S(T,H) \cong Nk \left[\ln(2J+1) - \frac{1}{2} \frac{CH^2}{T^2} \right] \tag{1.11a}$$

For a ferromagnet above its Curie temperature the analogous equation is valid

$$S(T,H) = Nk\left[\ln(2J+1) - \frac{1}{2}\frac{CH^2}{(T-T_C)^2}\right] \qquad (1.11b)$$

In a completely disordered state (H = 0, T $\rightarrow \infty$) the second term in the above equations (1.11) approaches zero, and the magnetic entropy of the system with localized magnetic moments reaches its maximum value

$$S_M = Nk_B \ln(2J+1) \equiv R\ln(2J+1) \qquad (1.12)$$

where R is the universal gas constant. This value represents the theoretical upper limit of the entropy that can be utilized in the MCE. The magnetic entropy associated with magnetic ordering varies from ~60% to ~90% of this theoretical limit. Part of the missing entropy is associated with spin fluctuations (5% to 15%) above T_C, while crystalline electric fields effects (CEF) may account for a major portion of the rest of missing entropy [6].

The magnitude of the magnetic entropy change ΔS_M with the change of magnetic field can be calculated from the Maxwell relation from magnetization data as:

$$\Delta S_M = S_M(H_2,T) - S_M(H_1,T) = \int_{H_1}^{H_2}\left(\frac{\partial M(H,T)}{\partial T}\right)_H dH \qquad (1.13)$$

Using the equations for the Curie-Weiss law, equation (1.8) the values of ΔS_M for a paramagnet and for a ferromagnet above T_C can be calculated respectively as:

$$\Delta S_M \cong -\frac{1}{2}\frac{C\Delta(H^2)}{T^2} \qquad (1.14a)$$

$$\Delta S_M \cong -\frac{1}{2}\frac{C\Delta(H^2)}{(T-T_C)^2} \qquad (1.14b)$$

where $\Delta(H^2) = H_2^2 - H_1^2$. As one can see from the above equations large values of ΔS_M are expected in magnetic materials with large M_{eff} and in a temperature range close to 0K for paramagnets and close to T_C for ferromagnets.

In paramagnets the lattice contribution to the heat capacity is negligibly small at temperatures close to absolute zero. At higher temperatures where the lattice heat capacity of the paramagnet is large the small generated MCE heat is absorbed by the lattice degrees of freedom of the solid and practically no temperature change can be observed. In ferromagnets there are two opposite forces, i.e. the ordering force due to exchange interaction of the magnetic moments, and the disordering force of the lattice thermal vibrations, are approximately balanced near the T_C. Hence, the isothermal application of a magnetic field produces a much greater increase in the magnetization (i.e. an increase in magnetic order and consequently, a decrease in magnetic entropy, ΔS_M) near the Curie point than far away from it. The effect of magnetic field above and below T_C is significantly reduced because only the paramagnetic response of the magnetic lattice can be achieved for $T >> T_C$, and for $T << T_C$ the spontaneous magnetization is already close to saturation and can not be increased much more.

In the ferromagnetic state the calculation of magnetic entropy change, ΔS_M, can be done by solving the magnetization equation (1.7), then using the Maxwell equation (1.2), and equation (1.13) to obtain ΔS_M. Since equation (1.7) has only numerical solution, the integration in equation (1.13) can be done only numerically.

1.2 Magnetic refrigeration and materials

More than 40 years after its discovery, the practical use of magnetocaloric effect was suggested independently by Debye [7] and Giauque [8] to reach ultra-low temperatures in a process called adiabatic demagnetization. This was a simple one step cooling process. Since the 1950's a few continuous magnetic refrigerators operating at various temperatures from ~1 to ~30 K have been constructed and tested. But most were inefficient and were run for only a few days at most.

Recently a study by Astronautics Corporation of America and the Ames Laboratory has proven that sub-room temperature active magnetic regenerator magnetic refrigeration is indeed energy efficient and is competitive with the gas compression technology [9]. The demonstration unit uses Gd as the regenerator/refrigerant. A record cooling power of 600 Watts in field of 5 T was obtained, which is 100 times better than previous near room temperature magnetic refrigerators. Its efficiency approaches 60% of Carnot efficiency at 5 T with a coefficient of performance (which is defined as cooling power divided by input power) approaching 15. The maximum temperature span reached is 38K.

Materials used in magnetic refrigerators should be soft ferromagnetic materials with large MCE and appropriate ordering temperature. Soft magnetic materials are used to reduce the hysteresis losses. A large MCE value will increase COP of the refrigerator. Most of the research on the MCE has been associated with materials ordering from ~4 to ~77 K for applications such as helium and hydrogen liquefaction, or materials ordering near room temperature for applications such as conventional air conditioning and refrigeration.

A typical ferromagnet undergoes a second order magnetic phase transition upon cooling from a paramagnetic state. A maximum appears near the transition temperature in the MCE plot. Such materials exhibit "caret"-like MCE behavior. Similar behavior can be found in a number of systems, such as Gd, $Gd_{1-x}R_x$(R = Dy, Ho, Er and Y), $GdAl_2$, $HoAl_2$, some of the $(Dy_{1-x}Er_x)Al_2$ alloys, GdPd, RNi_2(R = Gd, Dy and Ho), and the Mn perovskites.

There are also many materials that exhibit two or more magnetic phases as a function of temperature at zero magnetic field. These include most lanthanide metals and many intermetallic phases [10, 11]. For some materials of this kind the magnetic transitions occur at temperatures sufficiently far apart so that the MCE peaks do not appreciably overlap. One example of this class is GdMnSi which has three widely spaced magnetic transitions at ~50K, ~275K and >325K. The MCE plot of GdMnSi shows one minimum and two maxima near the transition temperatures, respectively. In other materials the transitions are close enough for the MCE of two or more magnetic phases to overlap. One of the extensively studied materials of this kind is $(Gd_{1-x}Er_x)NiAl$ [12]. The number of magnetic phases in this series varies from one to four. For the $(Gd_{0.60}Er_{0.40})NiAl$ four magnetic transitions were found at 16K, 29K, 34.5K and 43.5K. These transitions are so close to each other that they can not be distinguished from each other. As a result $(Gd_{0.60}Er_{0.40})NiAl$ exhibits a flat "table-like" MCE. This kind of materials is suitable for refrigeration devices utilizing an Ericsson cycle [13], which for optimum efficiency, the entropy-temperature curves for the magnetic refrigerant must be parallel between the minimum and maximum operating temperatures, i.e., ΔS_M must be constant for the full

temperature span of the cycle. However, the relatively low ΔT_{ad} value will be a limiting factor in the utilization of the RNiAl phases in cooling applications.

The major breakthrough for the study of MCE came with the discovery of giant MCE in $Gd_5(Si_xGe_{1-x})_4$ alloys where $0 \leq x \leq 0.5$ [14]. These alloys have a first order magnetic transition which brings about the giant MCE. The transitions in alloys with $0.24 \leq x \leq 0.5$ are also accompanied by crystal structure transformation. The temperature of the giant MCE is easily tunable between ~30 and ~275K by changing the Si:Ge ratio. Furthermore, by alloying with Ga, the giant MCE temperature increases to ~290K. The reversible magnetic field induced magnetic entropy change, ΔS_M, and the adiabatic temperature rise, ΔT_{ad}, for a low to moderate magnetic field change (0 to 2-10T) are the largest ever observed at the corresponding Curie temperatures. The ΔS_M is 100% to 400%, and the ΔT_{ad} is 25% to 200% larger than that for the best known prototypes. The improved MCE properties and refrigeration capacity should lead to increased performance and efficiencies, thus making magnetic refrigeration even more competitive with conventional gas-compression technology and opening the door for small-scale applications in appliances.

1.3 Rationale

The requirements for magnetic refrigeration materials include large MCE values to improve the coefficient of performance and an appropriate magnetic transition temperature at which maximum MCE peaks can be found.

Generally 4f metals (lanthanides) and their alloys are chosen rather than 3d metals and their alloys because the available theoretical magnetic entropy in the former is considerably larger than in the latter. The rare earth metals form a sub-group in the periodic table in which the 4f shell is progressively filled from La to Lu with the 5s, 5p and 6s shells already filled. The magnetic properties are associated with the partly filled 4f shell.

Gd has 7 4f electrons, with fairly large magnetic entropy of 17.3J/g-at K. For comparison the magnetic entropy of iron metal is 7.3J/g-at. Fe K, which is nearly 2½ times smaller than that of gadolinium. The ordering temperature of Gd is 294K, which is near room temperature. Furthermore, crystal electric field (CEF) effects can limit the magnetocaloric effect. Only for gadolinium-based materials, one does not need to worry about CEF effects since it has a half-filled 4f level and thus a spherical 4f electron cloud and no CEF can occur. Therefore, Gd and its alloys are ideal candidates for applications of near room temperature refrigeration.

In order to explore the materials with ordering temperatures in the vicinity of room temperature, we studied the magnetothermal properties of the $Gd_4(Bi_xSb_{1-x})_3$ alloy series. These alloys order in the temperature range of 260K to 340K [15]. Therefore they might be potential candidate magnetic refrigeration materials for near and slightly above room temperature applications such as air conditioners for home and automobiles, home refrigerator/freezers, etc.

2. EXPERIMENTAL PROCEDURES

2.1 Sample preparation

A total of five alloys with the $Gd_4(Bi_xSb_{1-x})_3$ stoichiometry with x ranging from 0 to 1 were prepared by melting the mixture of pure components in an induction furnace after the individual elements were sealed in tantalum crucibles in an atmosphere of helium. The gadolinium was prepared by the Materials Preparation Center of the Ames Laboratory and was 99.9 at.% pure with the major impurities as follows: C-0.080, O-0.010, F-0.006, Fe-0.004, Al-0.004, where the number after the chemical symbol represents impurity content in atomic percent. The bismuth and antimony, which were purchased from CERAC, Inc., were 99.999 wt.% pure. Each alloy was melted three times, turning the crucible over each time after re-melting to ensure the homogeneity of the alloys.

Initially all the alloys were melted at 1900°C, which is the highest temperature that can be measured by the thermocouple available. X-ray examination indicated there are at least two phases present in all the samples containing antimony. Subsequent heat treatment did not eliminate the second phases. According to the Gd-Sb phase diagram, Gd_4Sb_3 melts incongruently at 1770 °C, forming αGdSb and the melt. αGdSb transforms to βGdSb at 1840 °C which melts at 2130 °C. This means that a second phase with a melting point higher than 1900°C will form when all the components are melted. Therefore, higher temperatures were used to melt the highest melting point phase in the Gd-Sb system. Temperatures as high as 2500°C were reached by extrapolating the power

and frequency reading of the induction furnace to the corresponding temperatures. This is to ensure that the temperature reaches above the highest melting point of all the phases in the alloy. The melting procedures are listed in Table 2.1.

X-ray examination showed that the resulting alloys were essentially single-phase materials. However, metallography revealed some second phase on grain boundary. Since the alloys were sealed in crucibles the weight losses after the melting were negligible and therefore, the alloy compositions were accepted as nominally prepared.

Table 2.1

$Gd_4(Bi_xSb_{1-x})_3$	x=1	x=0.75	x=0.5	x=0.25	x=0
Procedure	1900 °C, 15min 1550 °C, 1hr	2500 °C, 15 min air quench	2500 °C, 15 min air quench	2500 °C, 15 min air quench	2500 °C, 15 min air quench

2.2 X-ray measurements

X-ray diffraction was used to confirm that the correct phase had been produced and to determine the lattice parameters of the materials. Diffraction analysis was performed on an automated Scintag powder diffractometer. The diffractometer was controlled by a computer and utilized Cu-K_α radiation. Samples for the diffractometer were prepared by grinding the materials into powder using a mortar and pestle. This powder was then sprinkled on a greased microscope slide which was attached to the diffractometer's sample holder. Each scan was made over the two-theta angular range of 10 to 90 degrees. The

diffraction peaks were indexed using CSD crystallographic software [16] on IBM compatible PC.

2.3 Magnetic measurements

The magnetic measurements were performed on an Oxford Instruments MagLab 2000 magnetometer. The accuracy of the instrument is claimed by the manufacturer to be better than or equal to 0.1%. The AC magnetic susceptibility was measured around the ordering temperatures of the respective alloys in an ac field of 1.25Oe at 125Hz frequency without and in various bias DC fields. The DC magnetic susceptibility was measured from ~4K to ~400K using the low temperature insert of the magnetometer, and from 400K up to 800K the measurements were performed using the high temperature insert.

For AC susceptibility measurements, a primary coil is excited by driving an AC current through it. Located inside the primary coil are two secondary coils, which have been carefully balanced, so that when there is no sample present in either coil, the coils produce identical signals. Thus, when the two signals are subtracted the result is zero. If a magnetic sample is introduced into one of the coils, the impedance of that coil is affected, and the voltage induced will differ from the no sample case. Now when the signals from the two coils are subtracted the resultant is no longer zero. The in and out of phase portions of the resultant are related to the real and imaginary parts of the AC susceptibility respectively by the following equations:

$$\chi' = \alpha X/mfH_{rms},$$

$$\chi'' = \alpha Y/mfH_{rms},$$

where α is a calibration coefficient, m is the mass of the sample, and the applied AC signal has an root-mean-square magnitude of H_{rms} and a frequency of f. X and Y are the in and out of phase components of the voltage, respectively.

For DC magnetization measurements, a sample is moved through a pair of pickup coils which induces a voltage proportional to the moment. This can be written as:

$$m = -\alpha \int v\, dt,$$

where m is the moment, α is a calibration factor, v is the voltage which is integrated with respect to time. The mass magnetization can then be found by dividing the moment by the mass of the sample.

In order to measure the magnetocaloric effect magnetization isotherms were measured around the magnetic ordering temperatures with each isotherm being 5K apart and the magnetic field step being 0.2T within the isotherms. The magnetocaloric effect was then calculated from magnetization data numerically by integrating the Maxwell equation using the trapezoidal rule [17].

$$\begin{aligned} \Delta S_M(T_{av})_{\Delta H} &= \int_{H_I}^{H_F} \left(\frac{\partial M(H_{T_{av}})}{\partial T} \right)_H dH \\ &= \frac{\delta H}{2\delta T} \left(\delta M_1 + 2\sum_{k=2}^{n-1} \delta M_k + \delta M_n \right) \end{aligned} \tag{2.1}$$

where $T_{av} = (T_u + T_l)/2$ is the average of the temperatures of the two neighboring magnetic isotherms measured at T_u and T_l, $\delta T = T_u - T_l$ is the temperature difference between the two isotherms, δH is the constant magnetic field step within each isotherm, and n is the number of points measured for each of the isotherm. In this work $\delta H = 0.2T$ and $\delta T = 5K$.

2.4 Heat capacity measurements

The heat capacities at constant pressure as a function of temperature were measured using an adiabatic heat-pulse calorimeter under various fields. As the heat capacity and the entropy is related by the following equation

$$dS = \frac{C(T)_H}{T} dT \tag{2.2}$$

the total entropy was obtained by numerically integrating the above equation [17]

$$\begin{aligned} S(T_n)_H &= \int_0^T \frac{C(T)_H}{T} dT \\ &= 0.5\left\{ C(T_1)_H + \sum\left[\left(\frac{C(T_i)_H}{T_i} + \frac{C(T_{i+1})_H}{T_{i+1}} \right) \times (T_{i+1} - T_i) \right] \right\} \end{aligned} \tag{2.3}$$

Here H represent the magnetic field, and n is the number of heat capacity data points collected between T_1 and T_n. The term $C(T_1)_H$ accounts for the missing heat capacity data between the lowest temperature of the experiment, T_1 and $T = 0\,\mathrm{K}$ assuming that $C(T=0)_H = 0$.

Once the total entropy functions $S(T)_{H_I}$ and $S(T)_{H_F}$ are established, the $\Delta S_M(T)_{\Delta H}$ is calculated as the isothermal difference and the $\Delta T_{ad}(T)_{\Delta H}$ is calculated as the isentropic difference between the $S(T)_{H_I}$ and $S(T)_{H_F}$ functions

$$\begin{aligned} \Delta S_M(T)_{\Delta H} &= (S(T)_{H_F} - S(T)_{H_I}) \\ \Delta T_{ad}(T)_{\Delta H} &= (T(S)_{H_F} - T(S)_{H_I})_S \end{aligned} \tag{2.4}$$

3. RESULTS AND DISCUSSION

3.1 Crystal structure and metallography

The crystal structure of all of the $Gd_4(Bi_xSb_{1-x})_3$ alloys had been determined previously and reported in the literature [15]. The x-ray diffraction results of this study confirmed that the crystal structure is of the anti-Th_3P_4 type (space group $I\bar{4}3d$) for all the compounds tested. The lattice parameters are refined by full profile least square refinement and are shown in Table 3.1 together with the data from Ref. 15. The lattice parameters are plotted as a function of the concentration of Bi in Figure 3.1, together with the Curie temperature (see section 3.3). It can be seen from the figure that the lattice

Table 3.1. Lattice parameters [a]

Sample	a (Å)	
$Gd_4(Bi_xSb_{1-x})_3$	This study	Ref. 15
x = 0	9.2252 (6)	9.224
x = 0.25	9.2703 (6)	9.263
x = 0.5	9.3105 (6)	9.304
x = 0.75	9.3483 (5)	9.342
x = 1	9.3896 (4)	9.383

[a] Estimated standard deviation in the last significant digit is given in parentheses

parameter increases almost linearly with the Bi concentration. This is expected from the difference between the atomic radii of Bi (1.60Å) and Sb (1.45Å).

A metallographic examination of Gd_4Bi_3, see Figure 3.2, shows that the sample is essentially single-phased. However some second phase are seen in grain boundaries.

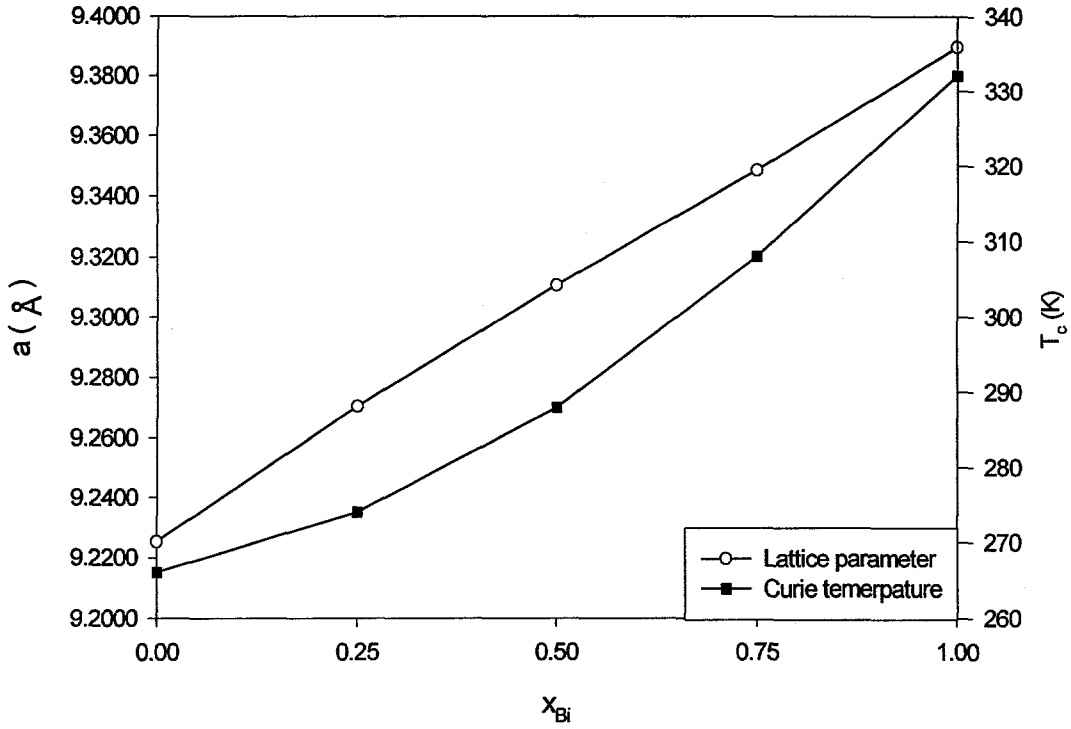

Figure 3.1 Lattice parameter as a function of Bi concentration

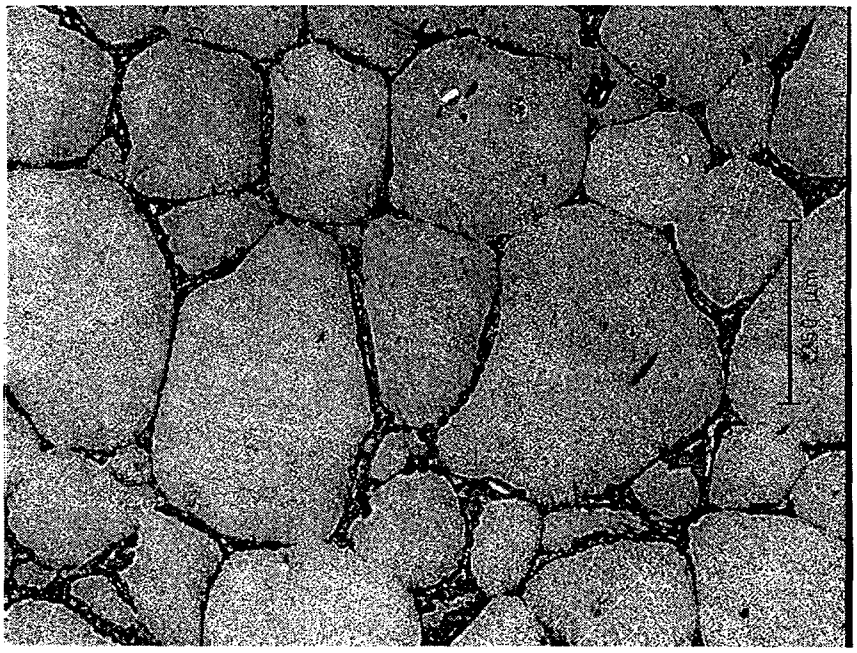

Figure 3.2 photomicrograph of Gd_4Bi_3, 100×

3.2 Magnetic measurements

3.2.1 DC magnetic susceptibility

The ordered magnetic moments of Gd_4Sb_3 and $Gd_4(Bi_{0.25}Sb_{0.75})_3$ were calculated from the low temperature saturation magnetization (T = 5K). The results are $7.37\mu_B$, and $7.28\mu_B$, respectively which are close to the theoretical value $7\mu_B$.

The inverse magnetic susceptibilities of the $Gd_4(Bi_xSb_{1-x})_3$ alloys are shown in Figure 3.3 for temperatures from 4K up to 800K. They all follow the Curie-Weiss law above their respective ordering temperatures.

The magnetic ordering temperatures and effective magnetic moments of the five alloys were calculated using the Curie-Weiss law from the measured data above the

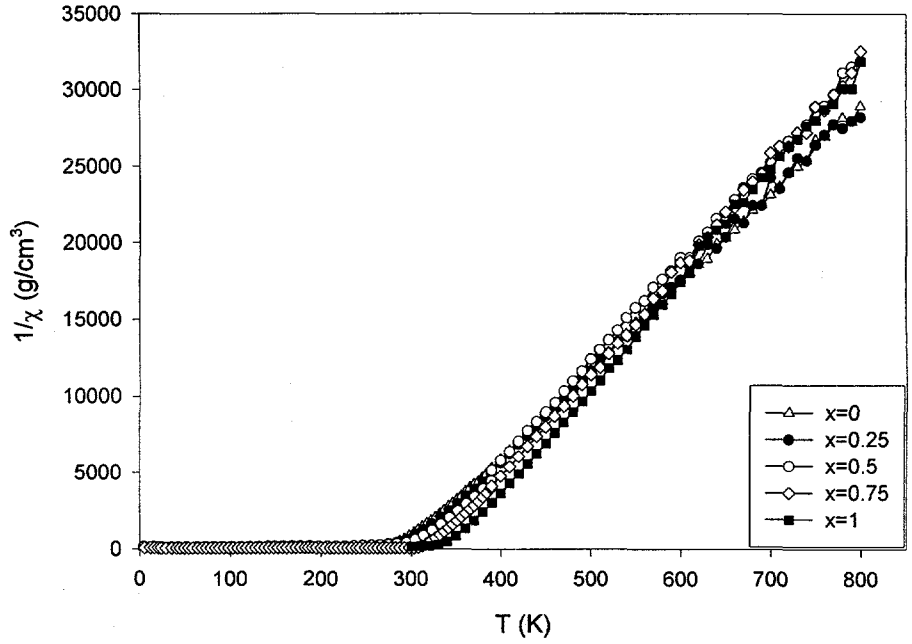

Figure 3.3 The inverse dc magnetic susceptibility of the $Gd_4(Bi_xSb_{1-x})_3$ alloys

ordering temperatures by least square regression of the equation:

$$\chi = \frac{C}{T - \theta_P}$$

The effective moment is obtained from

$$P_{eff} = 2.83\sqrt{MC}$$

where M is the molecular weight for a formula $Ga(Bi_xSb_{1-x})_{3/4}$ of the respective material.

The ordering temperatures and the effective magnetic moment per Gd ion of the $Gd_4(Bi_xSb_{1-x})_3$ alloys are listed in Table 3.2. It can be seen that the effective atomic magnetic moments per Gd ion in all alloys is lower than the theoretical value of $7.94\mu_B$ which corresponds to the zero orbital moment in the $^8S_{7/2}$ state of the 4f electrons.

The low temperature ordered magnetic moments being close to the theoretical value indicates that the ground state is truly ferromagnetic. However the paramagnetic effective moments are all much lower than the theoretical value. This is difficult to explain at present and needs further investigation.

Table 3.2 Curie-Weiss parameters

Sample $Gd_4(Bi_xSb_{1-x})_3$	θ_P (K)	P_{eff} (μ_B)	P_{eff} from Ref 15 (μ_B)	Ordered Magnetic Moment (μ_B) (T=5K)
x = 0	294	5.9	8.2	7.4
x = 0.25	300	6.0	8.1	7.3
x = 0.5	311	5.9	8.3	
x = 0.75	332	5.9		
x = 1	348	6.0	8.8	
Gd-metal		7.94		7

3.2.2 AC magnetic susceptibility

The real part of AC susceptibilities of the $Gd_4(Bi_xSb_{1-x})_3$ alloys in various DC bias fields are shown in Figures 3.4 – 3.8.

The figures show that all of the alloys exhibit a single magnetic transition and they are typical of a soft simple ferromagnet when we consider the curve of zero DC bias field. However the curves with non-zero DC bias fields show a peak near the Curie temperature. The peaks shifted to higher temperatures with increasing bias fields. Further investigation of the materials is needed to explain the nature of these peaks. It may also help to explain the low effective moment obtained in DC measurement.

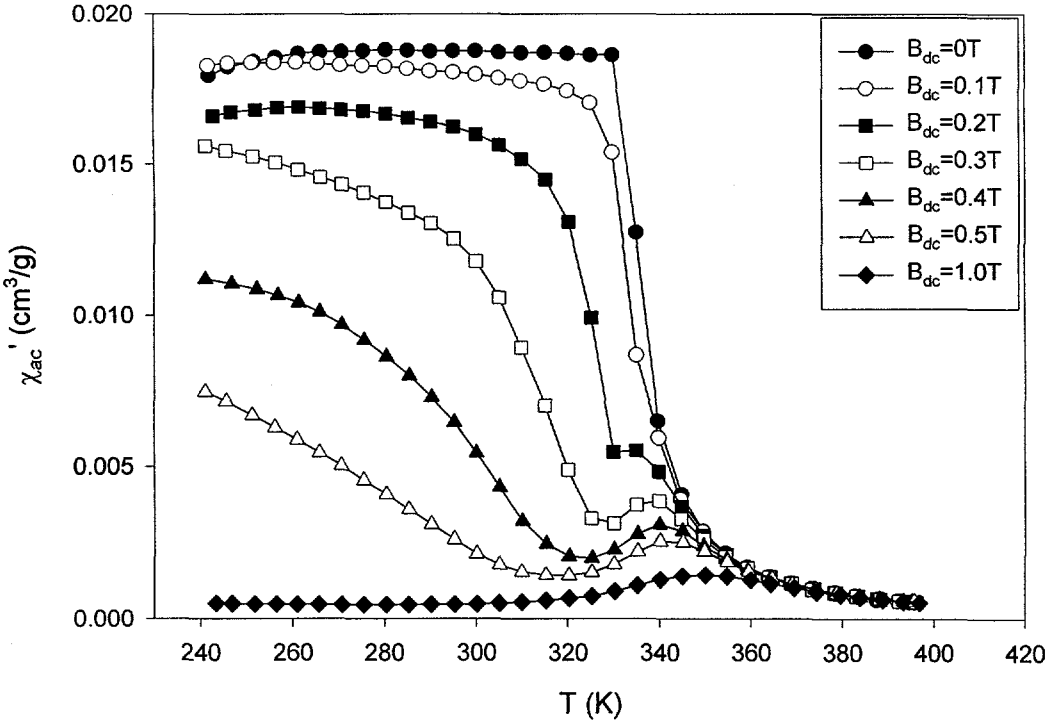

Figure 3.4 AC susceptibility for Gd_4Bi_3 at H_{ac}=1.25Oe, f=125Hz, ΔT=5K

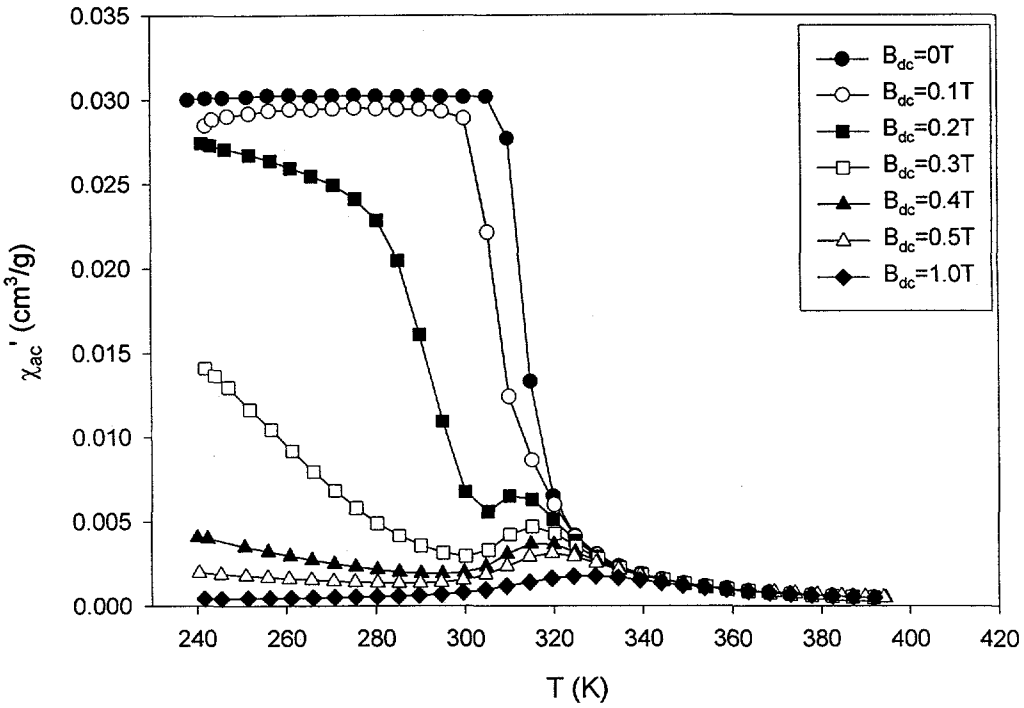

Figure 3.5 AC susceptibility for $Gd_4(Bi_{0.75}Sb_{0.25})_3$ at H_{ac}=1.25Oe, f=125Hz, ΔT=5K

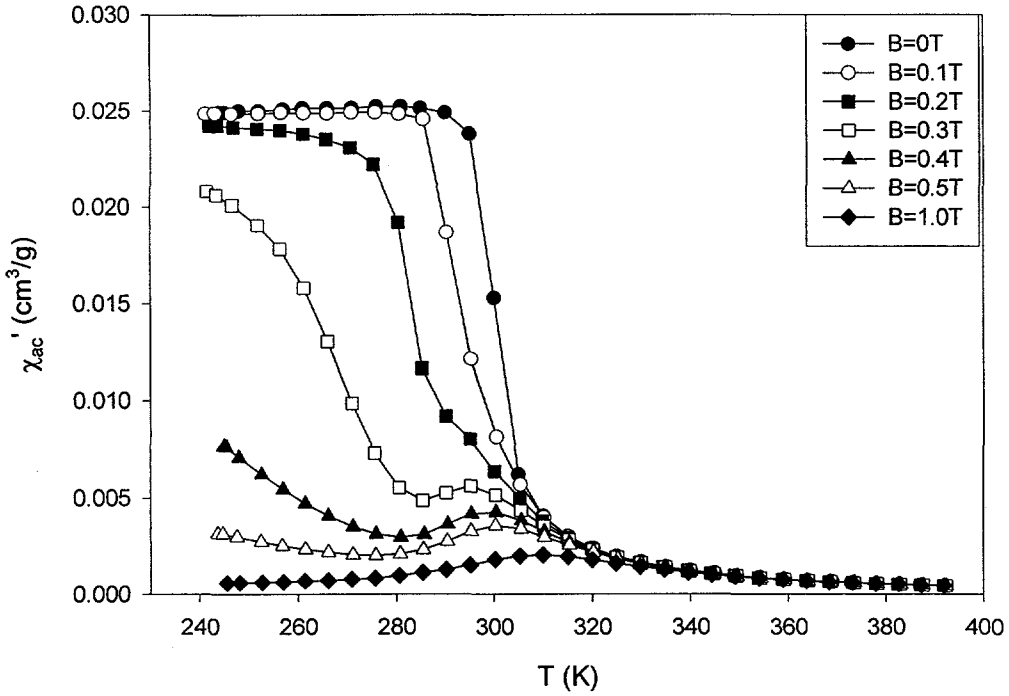

Figure 3.6 AC susceptibility for $Gd_4(Bi_{0.5}Sb_{0.5})_3$ at H_{ac}=1.25Oe, f=125Hz, ΔT=5K

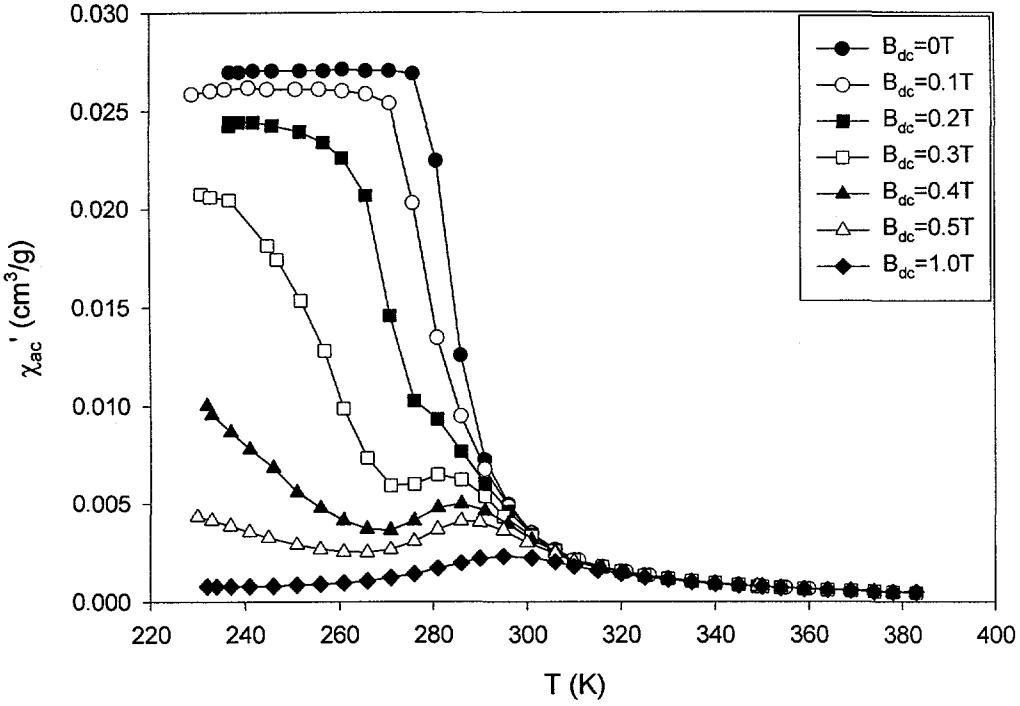

Figure 3.7 AC susceptibility for $Gd_4(Bi_{0.75}Sb_{0.25})_3$ at H_{ac}=1.25Oe, f=125Hz, ΔT=5K

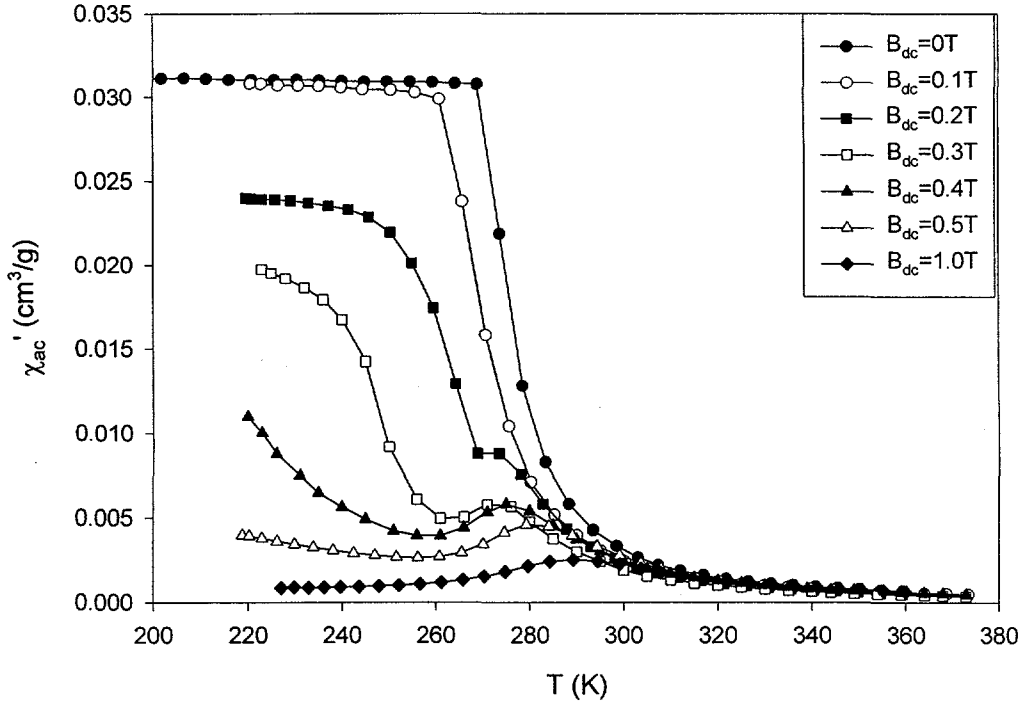

Figure 3.8 AC susceptibility for Gd_4Sb_3 at H_{ac}=1.25Oe, f=125Hz, ΔT=5K

The imaginary part of the AC susceptibility of $Gd_4(Bi_{0.25}Sb_{0.75})_3$ is shown in Figure 3.9. All the other alloys in the series have similar behavior and are not presented here. The imaginary part of the AC susceptibility of these alloys is quite extraordinary in that it shows negative values below the Curie temperatures. No explanations are available at present. The imaginary part of AC susceptibilities is always positive in the literature that can be found. No physical meaning can be associated with negative values. From the figure it is also reasonable to exclude experimental errors as the probable cause of the negative values because in paramagnetic region χ" is close to zero while in ferromagnetic region χ" is lower.

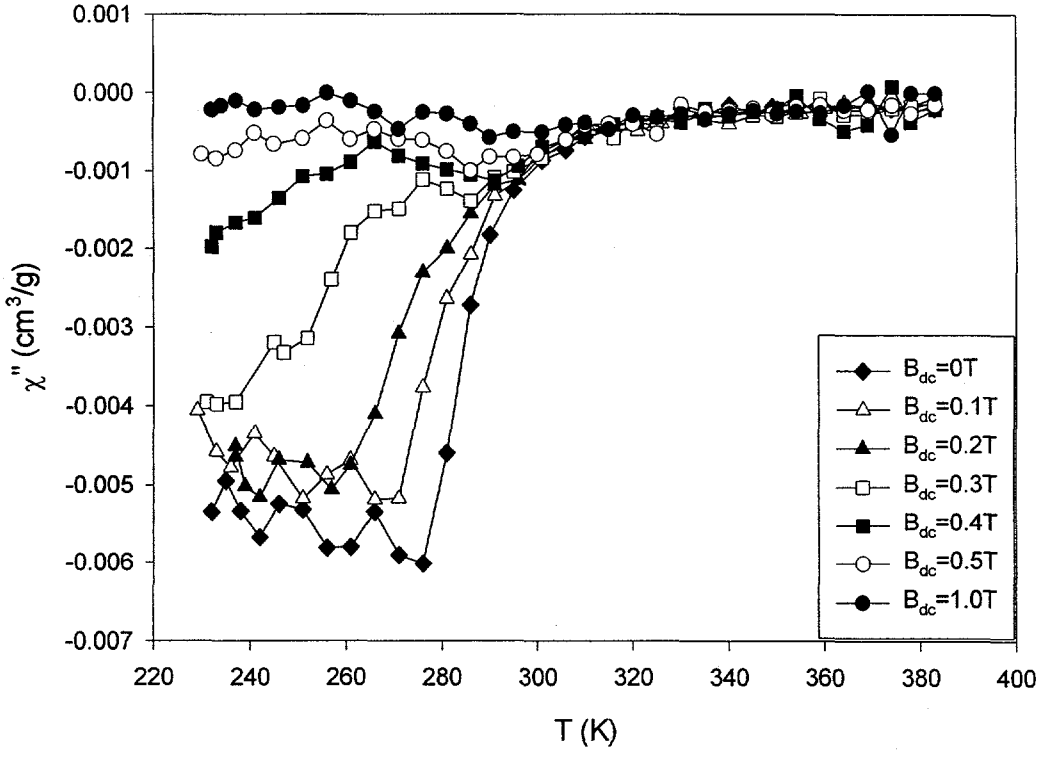

Figure 3.9 Imaginary part of AC susceptibility for $Gd_4(Bi_{0.25}Sb_{0.75})_3$ at H_{ac}=1.25Oe, f=125Hz, ΔT=5K

3.2.3 Magnetization measurements

The magnetization isotherms for the $Gd_4(Bi_xSb_{1-x})_3$ alloys, which were measured around their respective ordering temperatures every 5K and using a magnetic field step of 0.2T, are shown in Figures 3.10 - 3.14. The magnetization behavior is typical of those of simple ferromagnetic materials. These magnetization isotherms were then used to calculate the magnetic entropy change as a function of temperature for various magnetic field changes. The results are shown in Figures 3.15 – 3.19.

For all the alloys the magnetization at lower temperatures increases rapidly with magnetic field and then nearly saturates in a small magnetic field (< 5000Oe) indicating a ferromagnetic state. The magnetizations at higher temperatures are much lower than

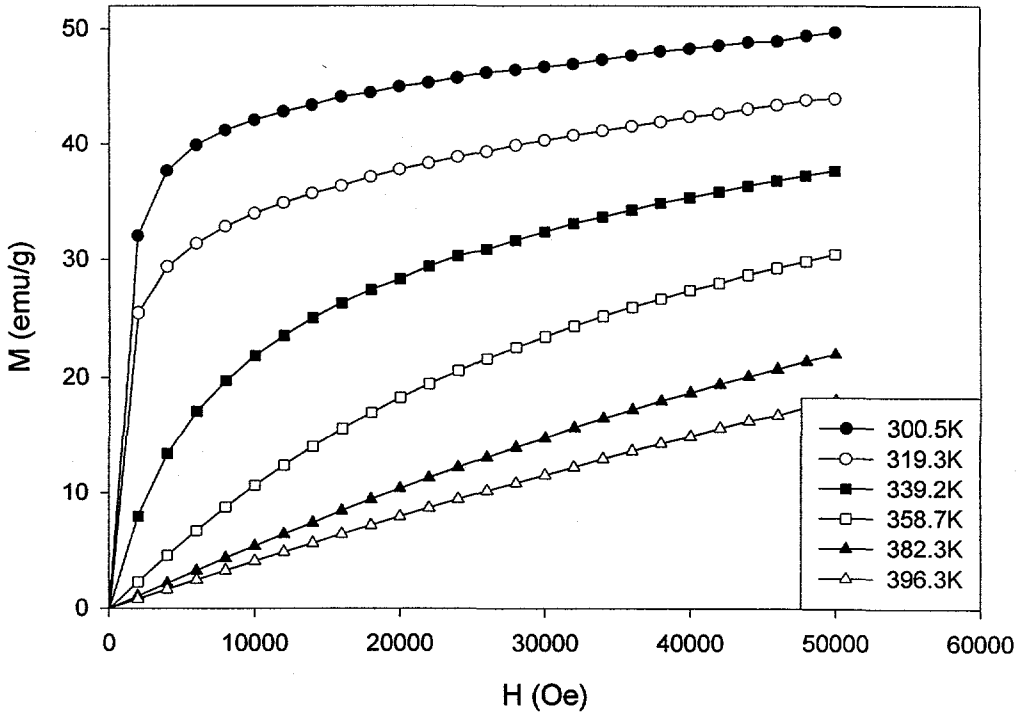

Figure 3.10 The magnetization isotherm of Gd_4Bi_3 as a function of magnetic field

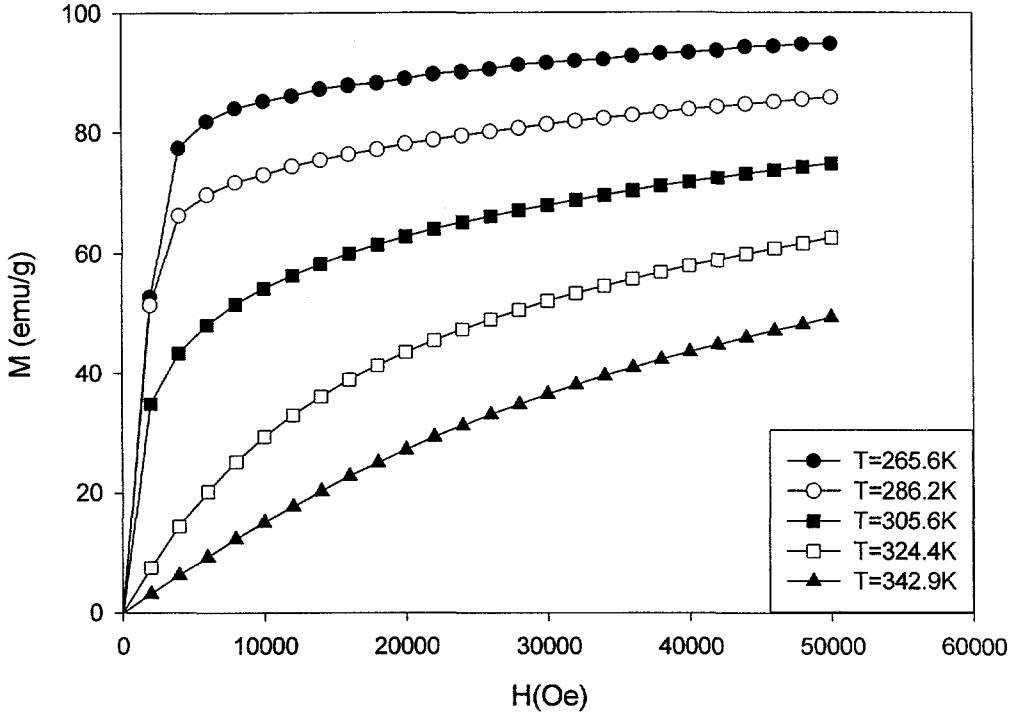

Figure 3.11 The magnetization isotherm of $Gd_4(Bi_{0.75}Sb_{0.25})_3$ as a function of magnetic field

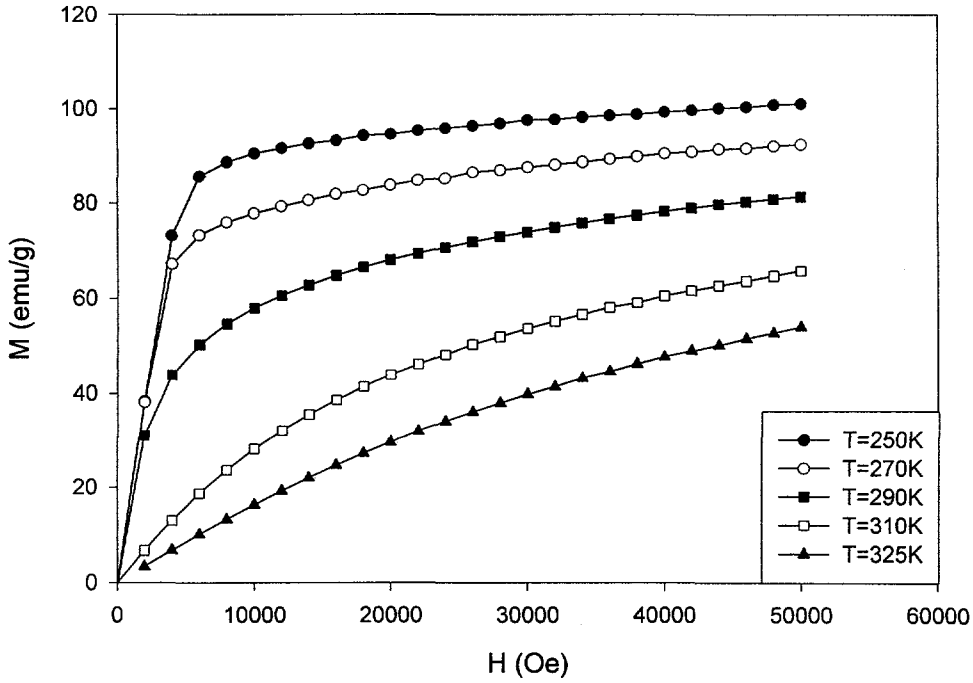

Figure 3.12 The magnetization isotherm of $Gd_4(Bi_{0.5}Sb_{0.5})_3$ as a function of magnetic field

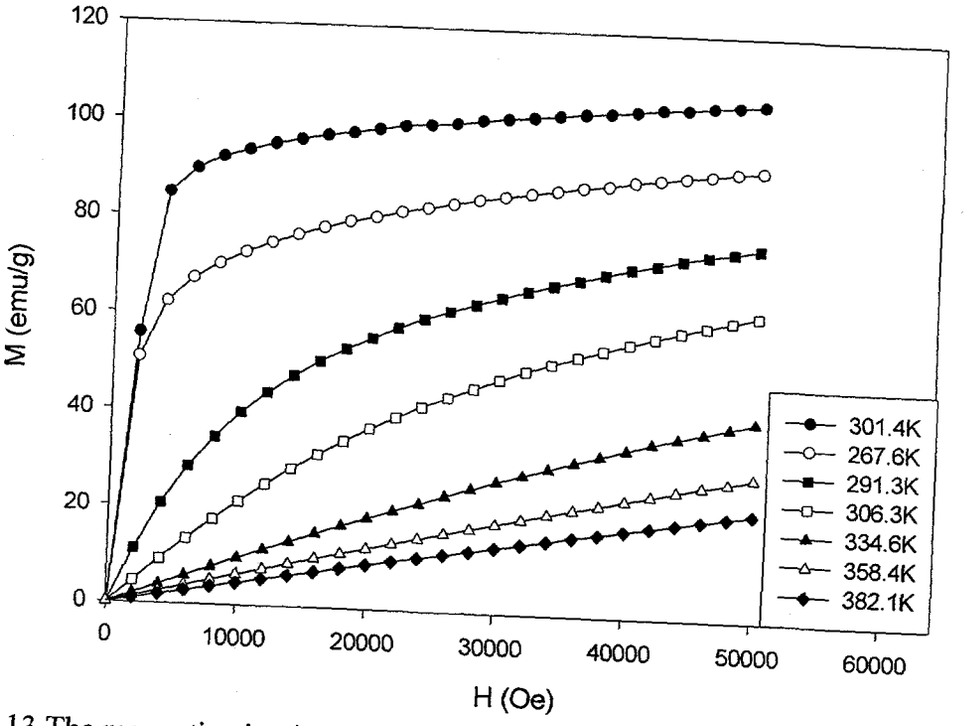

Figure 3.13 The magnetization isotherm of $Gd_4(Bi_{0.25}Sb_{0.75})_3$ as a function of magnetic field

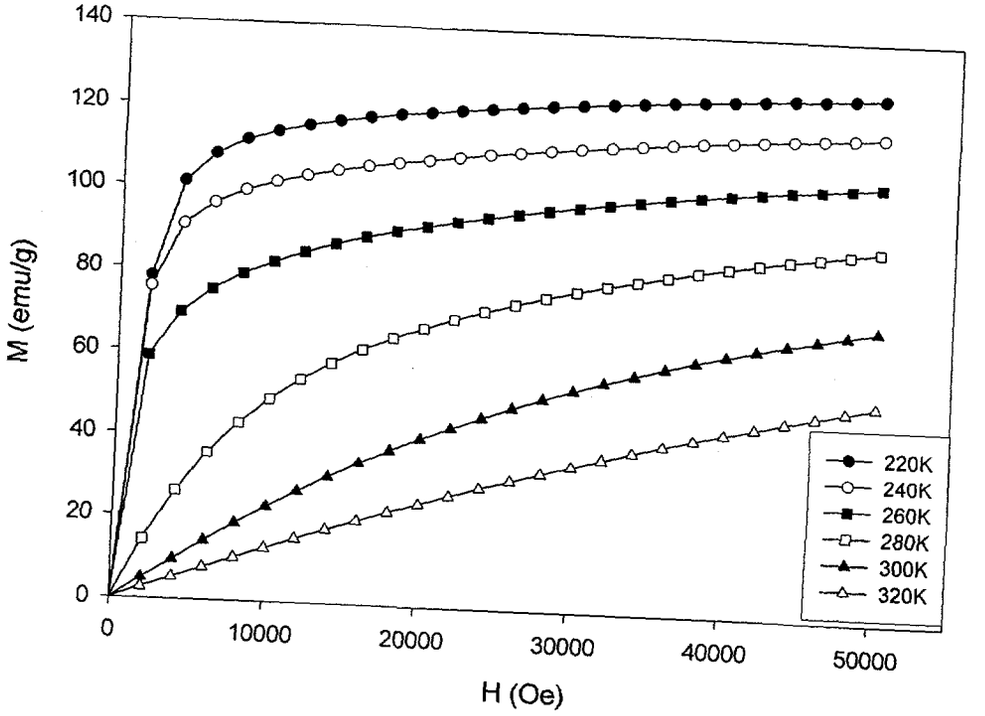

Figure 3.14 The magnetization isotherm of Gd_4Sb_3 as a function of magnetic field

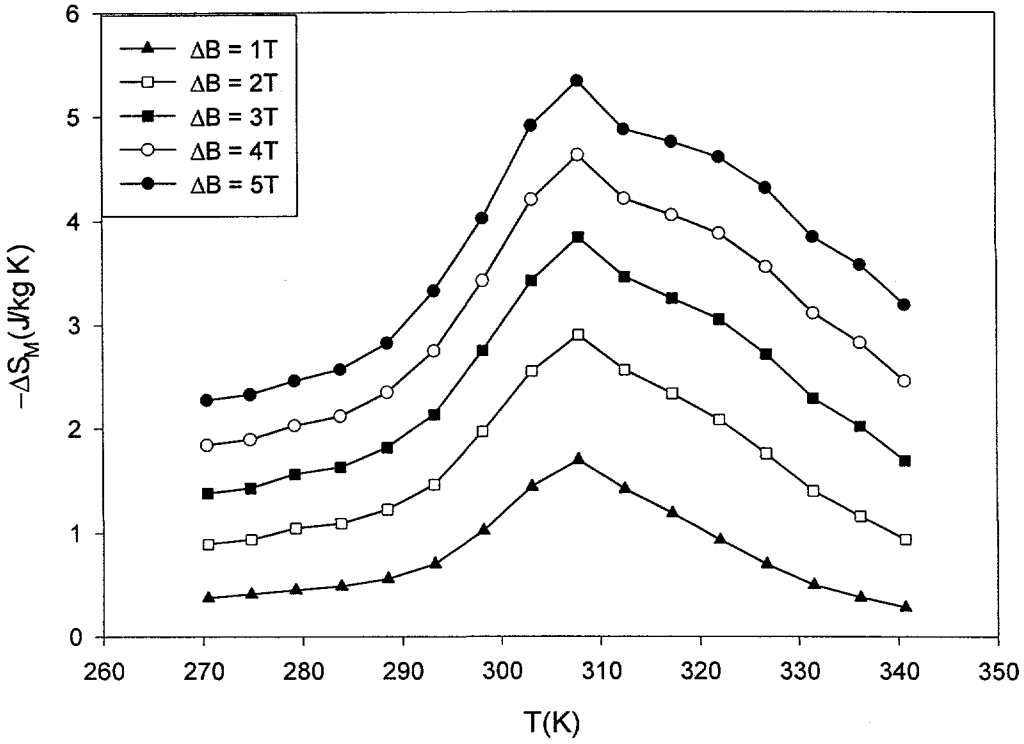

Figure 3.16 Magnetocaloric effect vs. Temperature for $Gd_4(Bi_{0.75}Sb_{0.25})_3$

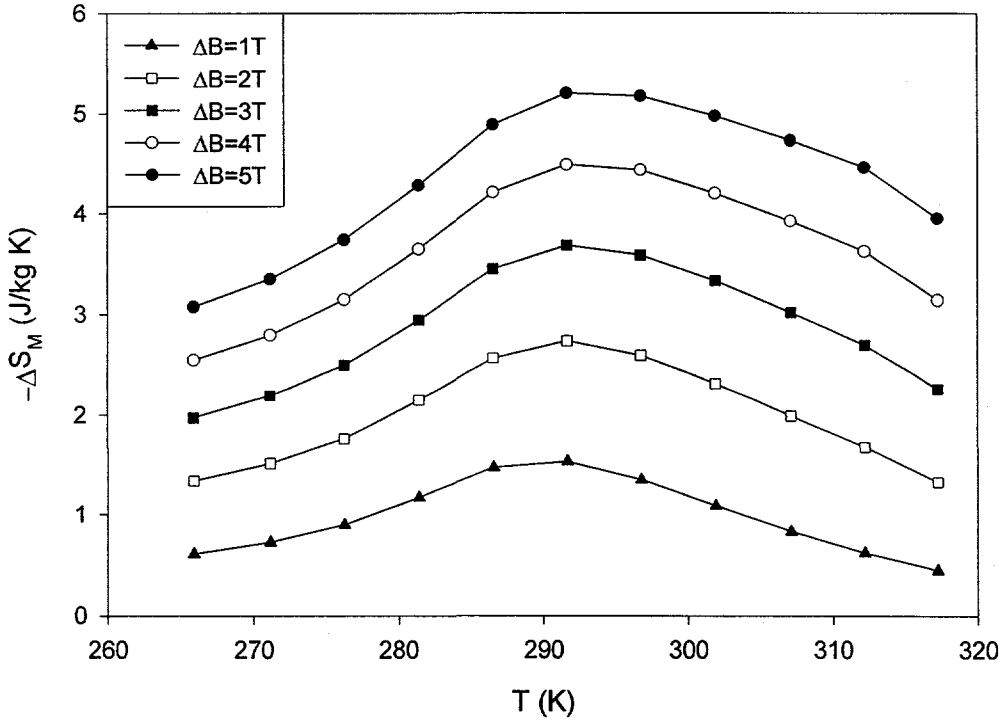

Figure 3.17 Magnetocaloric effect vs. Temperature for $Gd_4(Bi_{0.5}Sb_{0.5})_3$

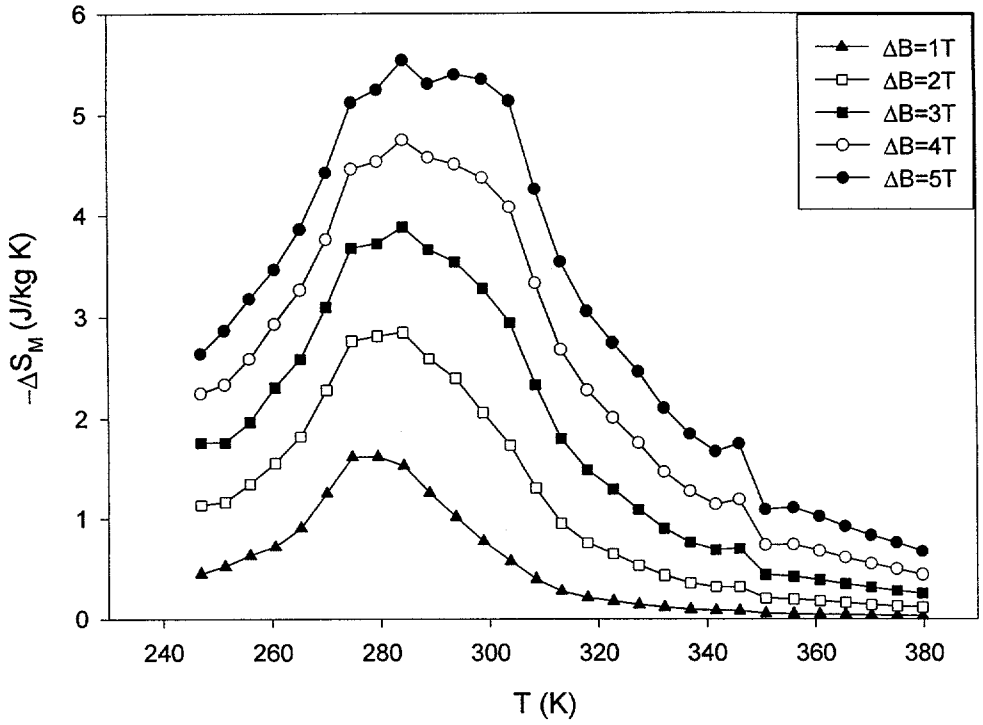

Figure 3.18 Magnetocaloric effect vs. Temperature for $Gd_4(Bi_{0.25}Sb_{0.75})_3$

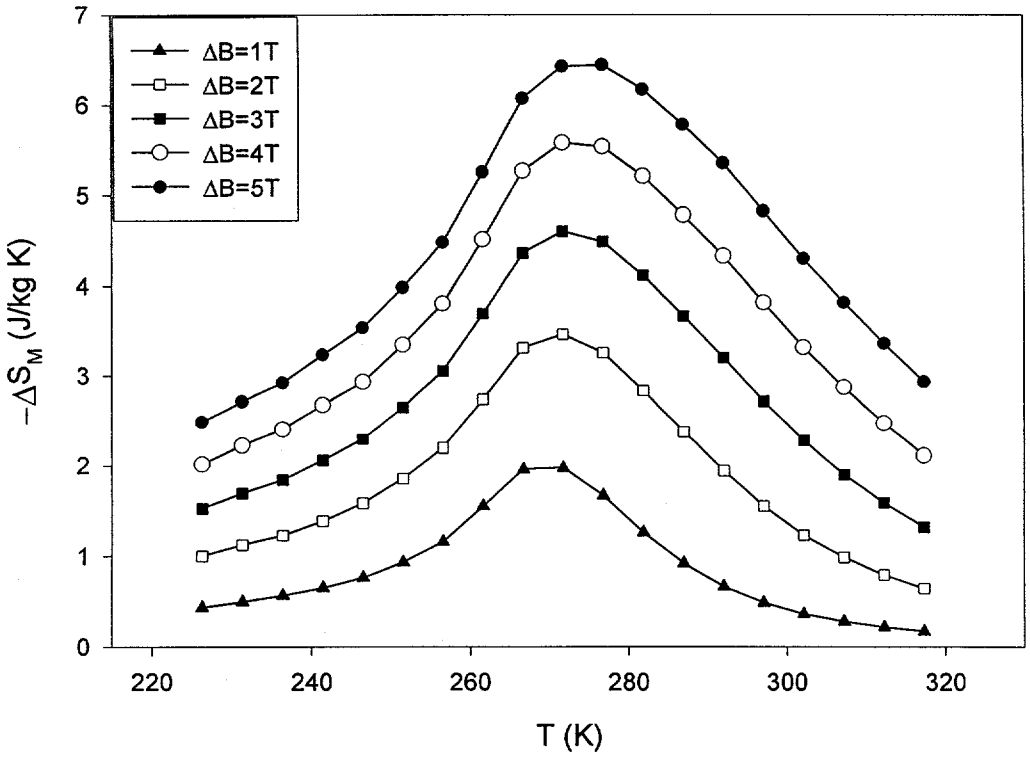

Figure 3.19 Magnetocaloric effect vs. Temperature for Gd_4Sb_3

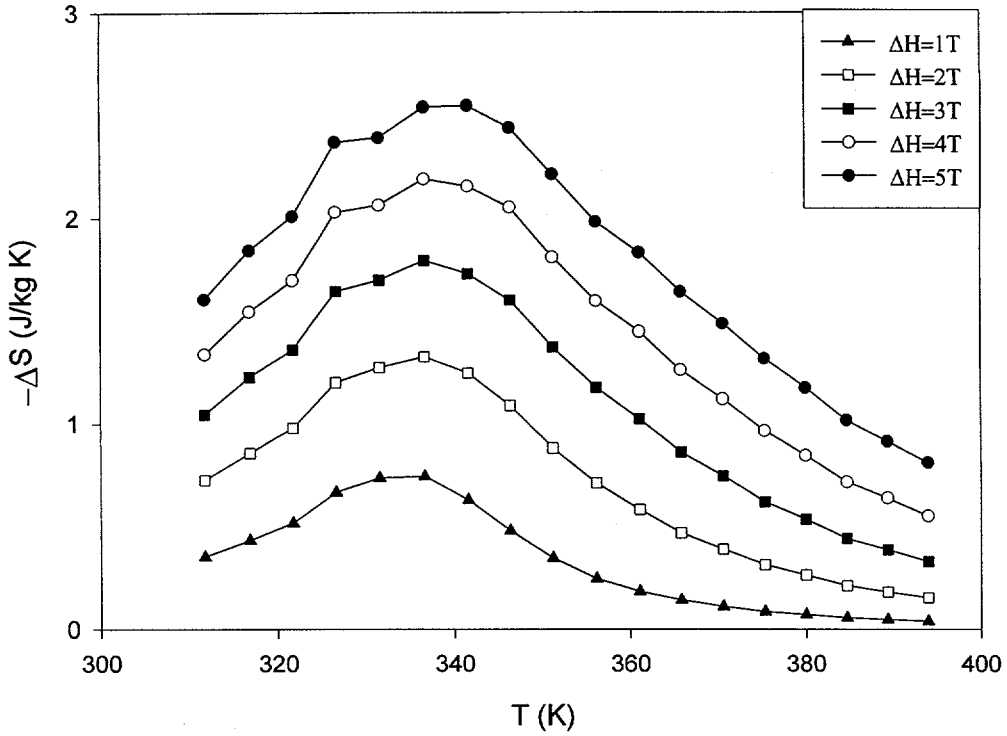

Figure 3.15 Magnetocaloric effect vs. Temperature for Gd_4Bi_3

those at lower temperatures and increase almost linearly with magnetic field, indicating a paramagnetic state. In a certain temperature region between the above two regions the difference between the neighboring isotherms is much larger indicating a spontaneous magnetic transition occurs in this temperature region. This is typical of a ferromagnet ↔ paramagnet transition. No other magnetic transitions were observed in this temperature region.

The magnetic entropy change calculated from the magnetization isotherms exhibit a single peak for $Gd_4(Bi_{0.75}Sb_{0.25})_3$, $Gd_4(Bi_{0.5}Sb_{0.5})_3$, and Gd_4Sb_3. The multiple peaks present in other alloys may be due to experimental errors as the accumulation of errors due to data processing when calculating the magnetocaloric effects can be as high as 10%

even at the Curie temperature where the accuracy should be the best [17]. Therefore the observed shape of the magnetocaloric effect curve needs to be verified by heat capacity measurements. However, it is clearly seen that the MCE peaks occur near the Curie temperatures of the respective alloys and the height of the peaks decrease with increasing Bi concentration, while the temperatures of the peaks increase with increasing Bi concentration. For each alloy of the series the MCE peaks move to higher temperatures with increasing magnetic field change.

3.3 Heat capacity measurements

The heat capacity under constant pressure was measured for all of the $Gd_4(Bi_xSb_{1-x})_3$ alloys under various magnetic fields. The zero magnetic field heat capacity of the five alloys are shown in Figure 3.20 and the heat capacity of Gd_4Sb_3 under various magnetic fields is shown in Figure 3.21. The magnetic field dependence of the heat capacity for the other alloys is essentially the same as that observed for Gd_4Sb_3 except for the temperatures of the peaks and will not be presented here.

The zero field heat capacity shows a single peak for each alloy. The heat capacity curve of Gd_4Bi_3 shows a little bump around 28K. This was attributed to the antiferro-magnetic transition of GdBi, which has a Néel temperature of 28K [18]. This is consistent with the microstructure shown in Figure 3.2, where a small amount of second phase material was observed in the grain boundary. The λ-shaped peak is indicative of a spontaneous magnetic ordering transition. It is a second order ferromagnet ↔ paramagnet transition. At high temperature the heat capacity of nonmagnetic materials approaches 3R, i.e. it approaches a constant value. In magnetic materials when the temperature

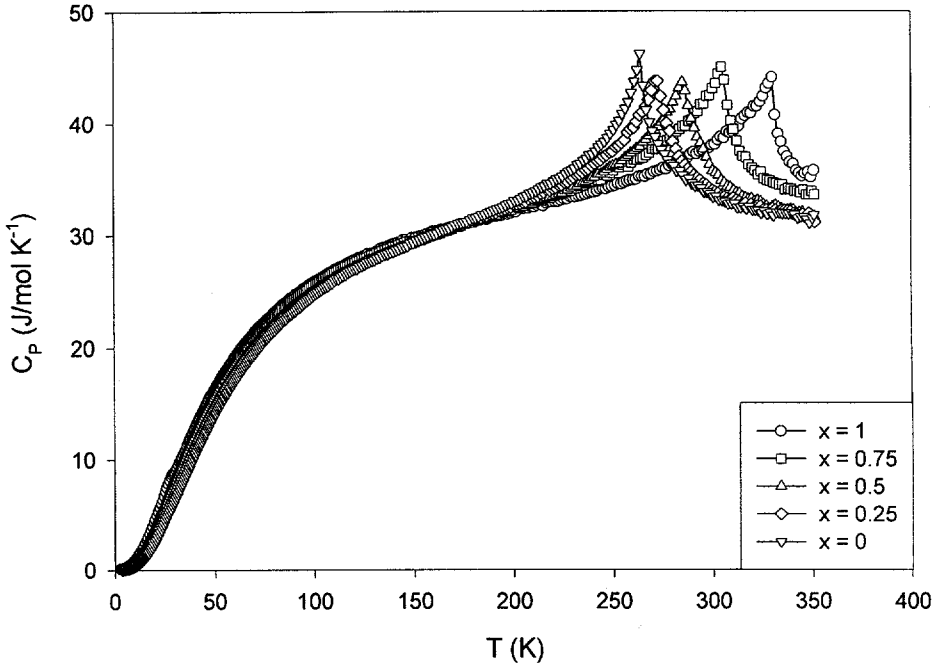

Figure 3.20 Zero field heat capacities of the $Gd_4(Bi_xSb_{1-x})_3$ alloys

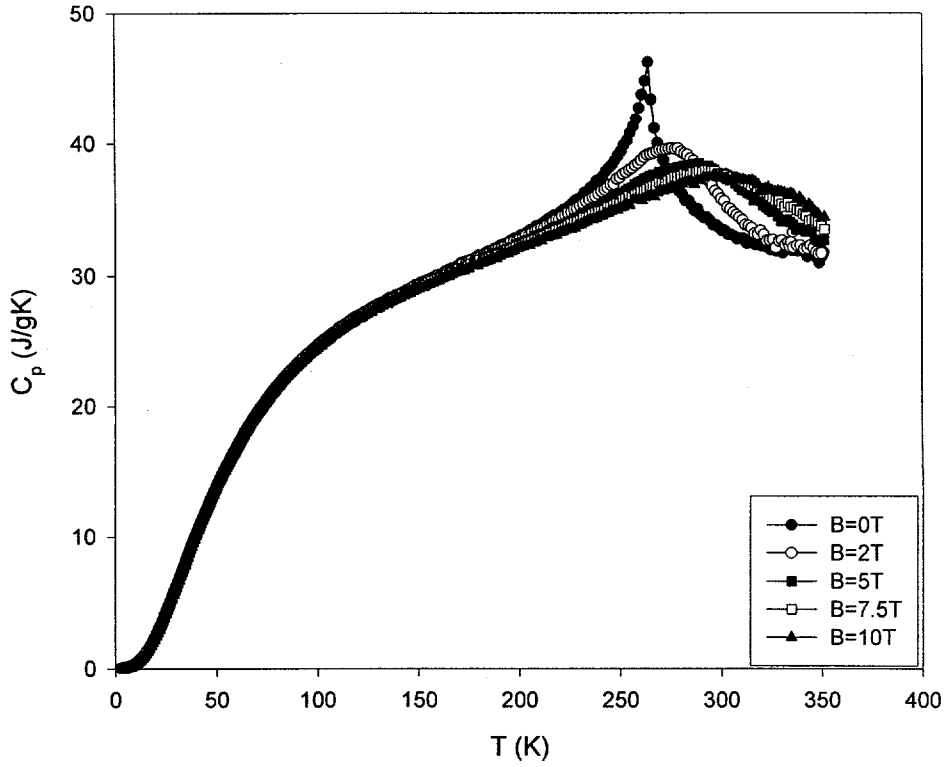

Figure 3.21 Heat capacities of the Gd_4Sb_3 alloys in various magnetic fields

approaches the Curie temperature upon cooling the magnetic interaction between the magnetic moments of the atoms begin to overcome the thermal energy to make them align parallel. This process absorbs energy causing the heat capacity to rise. At the Curie temperature a vast majority of the spins are suddenly aligned parallel due to exchange interaction, absorbing a great deal of heat which causes a sharp increase of the heat capacity. As the temperature is lowered the exchange interaction prevails and the degree of spin alignment gradually increases. As less heat is needed to align the magnetic spins the heat capacity drops until eventually the magnetic ordering process is complete and again only the lattice and electronic contributions to the heat capacity remain. The location of the transition temperature is the point where the maximum change of heat capacity with temperature occurs, i.e. the inflection point of the heat capacity curve on the high temperature side of the peak.

The temperatures of the heat capacity peaks in Figure 3.20 increase with increasing Bi concentration. This is consistent with the increasing magnetic ordering temperatures of the series with increasing Bi concentration. The magnetic ordering temperatures (Curie temperature) were determined from the inflection points of the zero field heat capacity curves, see Table 3.3.

Figure 3.21 is typical of the $Gd_4(Bi_xSb_{1-x})_3$ alloy series. The zero magnetic field heat capacity shows a typical λ-type maximum. When a magnetic field is applied the peak broadens and shifts to higher temperatures with increasing field strength. In the mean time the height of the peaks is greatly suppressed by the field. This is a typical behavior of a ferromagnet in the vicinity of the magnetic transition temperature. The effect of the

Table 3.3 Curie temperatures determined from heat capacity measurements

Sample $Gd_4(Bi_xSb_{1-x})_3$	Curie temperature (K)
x = 0	265.7
x = 0.25	274.4
x = 0.5	288.1
x = 0.75	307.7
x = 1	331.7

magnetic field is actually helping to align the magnetic moments of the atoms therefore the magnetic transition occurs at higher temperature overcoming the higher thermal energy that destroys the magnetic order. With the help of the external magnetic field the alignment of the magnetic moments takes less energy, therefore the height of the heat capacity peak is lowered.

The isothermal magnetic entropy change and the adiabatic temperature rise for all of the $Gd_4(Bi_xSb_{1-x})_3$ alloys for various magnetic field changes were calculated and the results are shown in Figures 3.22 – 3.26 and Figures 3.27 – 3.31, respectively. The magnetic entropy change for all of the alloys in the $Gd_4(Bi_xSb_{1-x})_3$ series exhibit a single caret-like maximum for all magnetic field changes measured. These peaks occur near the magnetic ordering temperature of the respective alloy. They do not coincide with the heat capacity maximum but always occur at temperatures a little higher. The peaks slightly move to higher temperatures with increasing magnetic field changes. The small anomalies in the low temperature regions of the entropy change curves are probably due to experimental errors since the heat capacities at these temperatures is very low so that uncertainty increases. However the negative anomaly around 28K in the magnetic

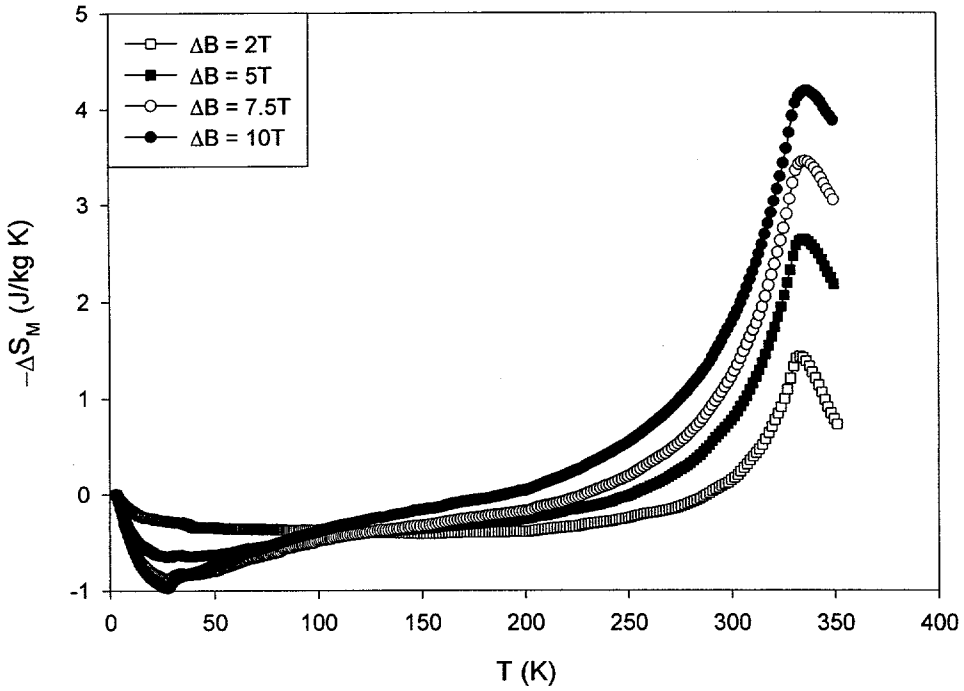

Figure 3.22 Entropy change for Gd_4Bi_3 for various magnetic field changes

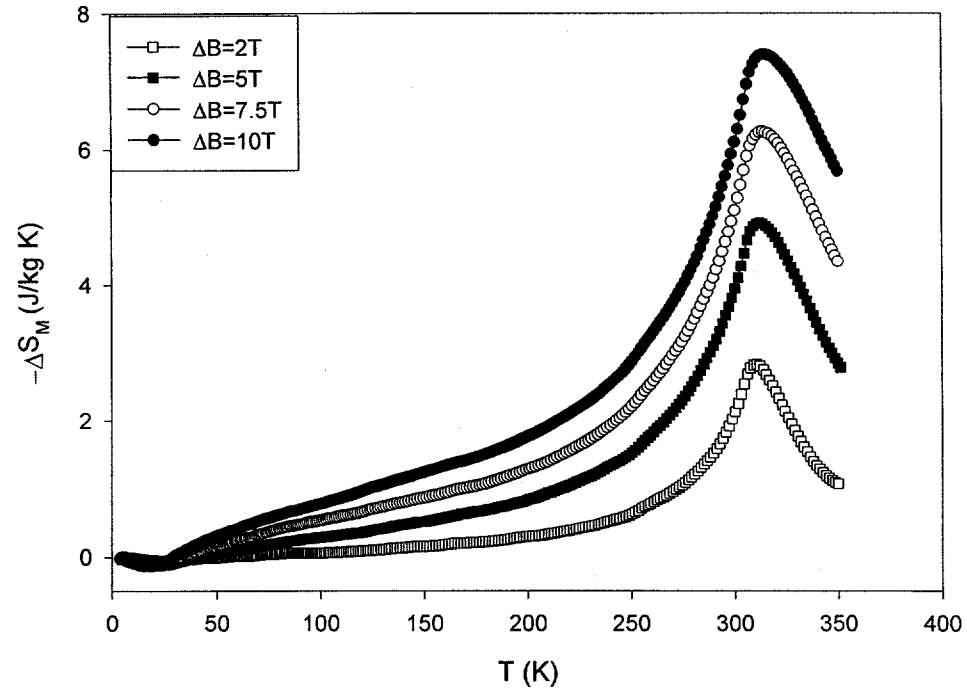

Figure 3.23 Entropy change for $Gd_4(Bi_{0.75}Sb_{0.25})_3$ for various magnetic field changes

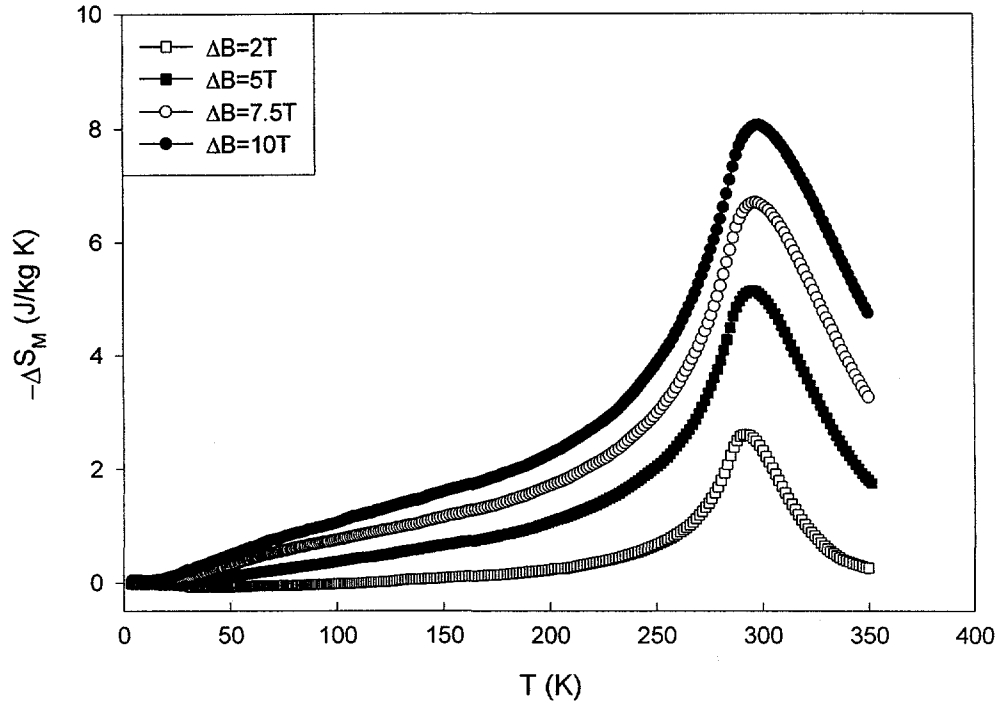

Figure 3.24 Entropy change for $Gd_4(Bi_{0.5}Sb_{0.5})_3$ for various magnetic field changes

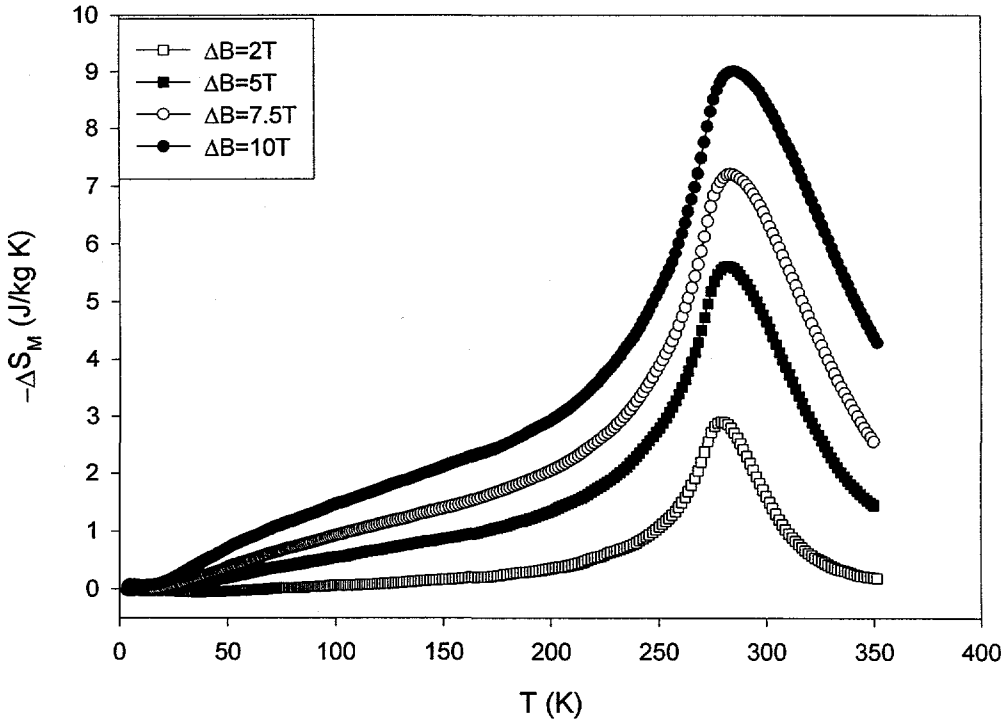

Figure 3.25 Entropy change for $Gd_4(Bi_{0.25}Sb_{0.75})_3$ for various magnetic field changes

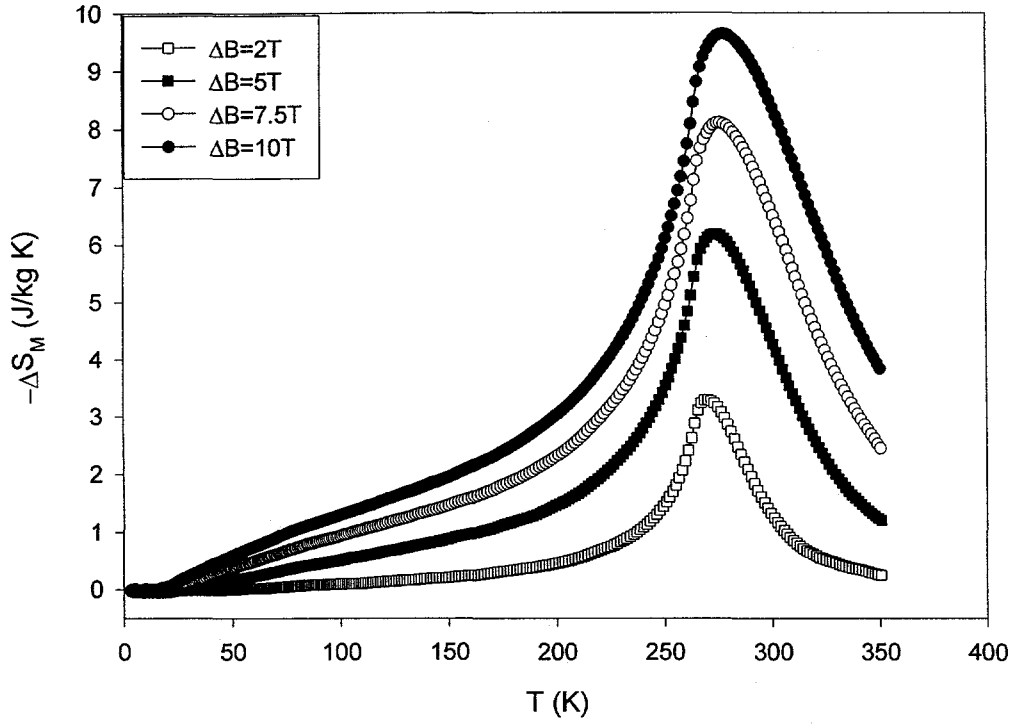

Figure 3.26 Entropy change for Gd_4Sb_3 for various magnetic field changes

entropy change in Gd_4Bi_3 is probably due to the antiferromagnetic transition of the GdBi impurity phase which was shown to be present in the sample in heat capacity measurements. In contrast to the effect of the magnetic field on a ferromagnetic transition, increasing the magnetic field for an antiferromagneitc transition will disrupt the antiferromagnetic coupling and increase the magnetic entropy. Thus the anomaly will be negative. This is also evident in the adiabatic temperature change which is negative for increasing field in Gd_4Bi_3, see Figure 3.27.

The adiabatic temperature rise exhibits a similar behavior to the isothermal magnetic entropy change. The MCE maxima occur near the magnetic ordering temperatures and correspond to the temperatures where the heat capacity of the magnetic material is not

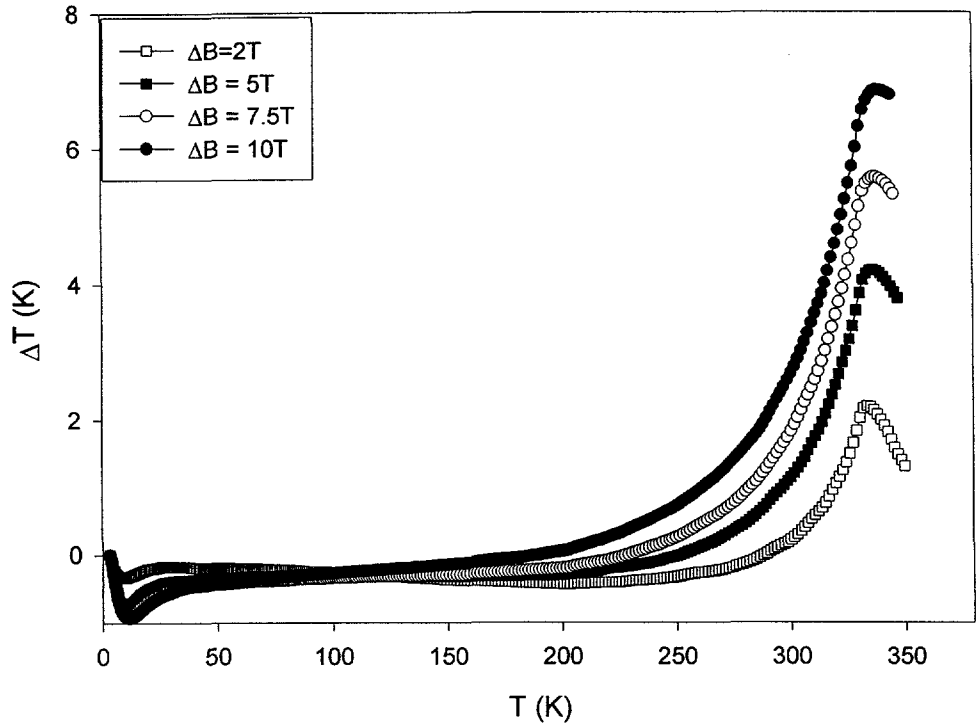

Figure 3.27 Temperature rises for Gd_4Bi_3 for various magnetic field changes

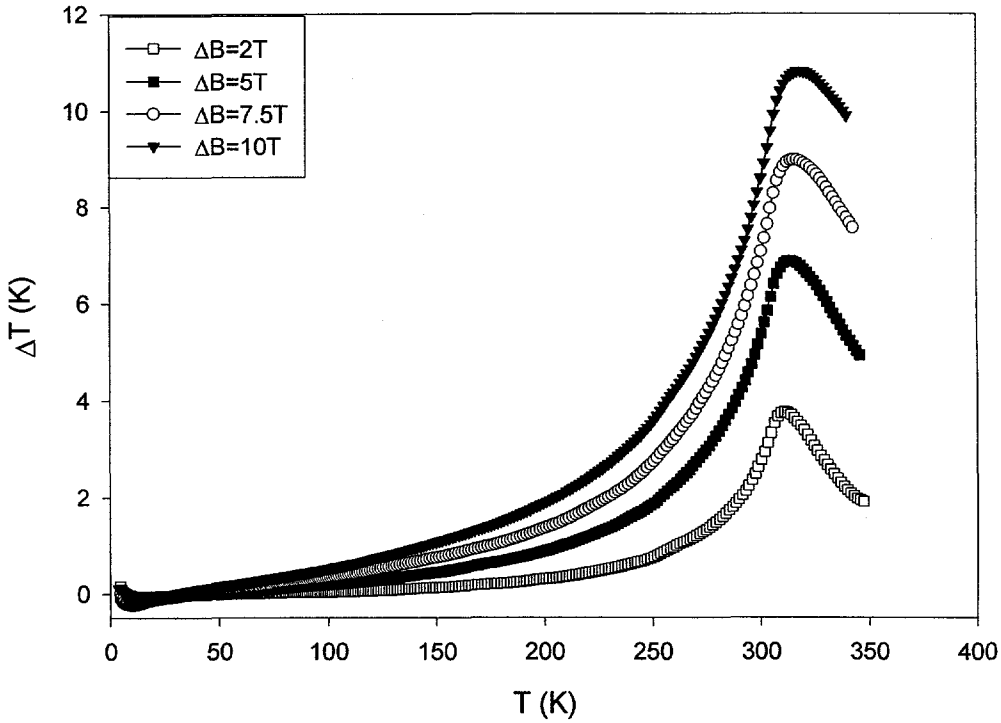

Figure 3.28 Temperature rises for $Gd_4(Bi_{0.75}Sb_{0.25})_3$ for various magnetic field changes

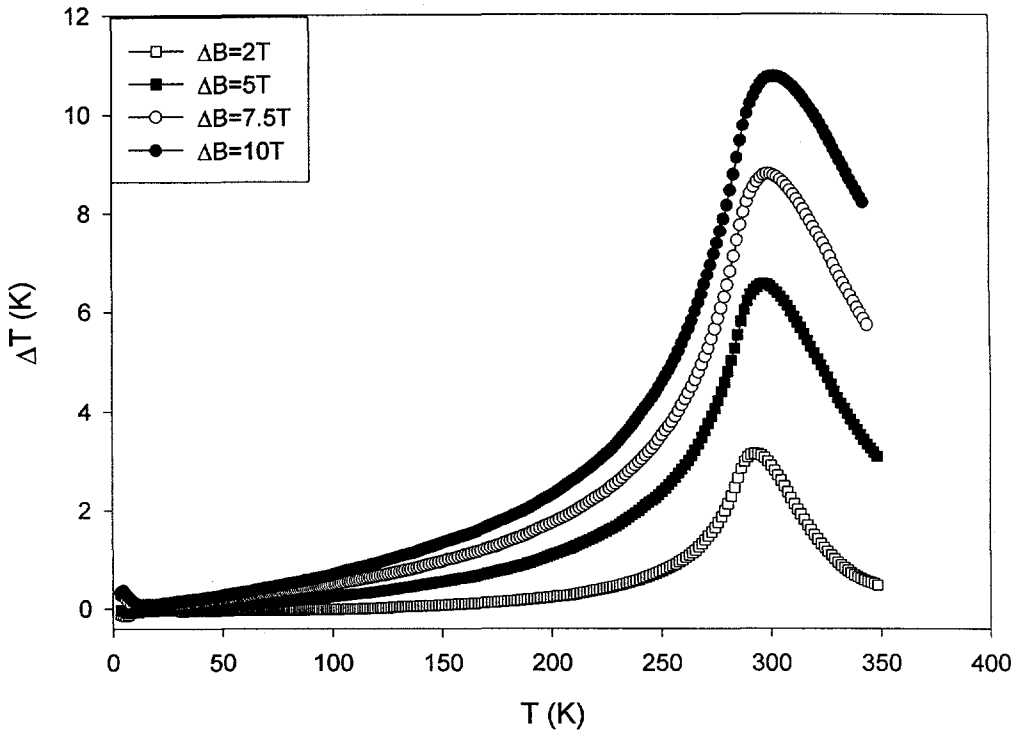

Figure 3.29 Temperature rises for $Gd_4(Bi_{0.5}Sb_{0.5})_3$ for various magnetic field changes

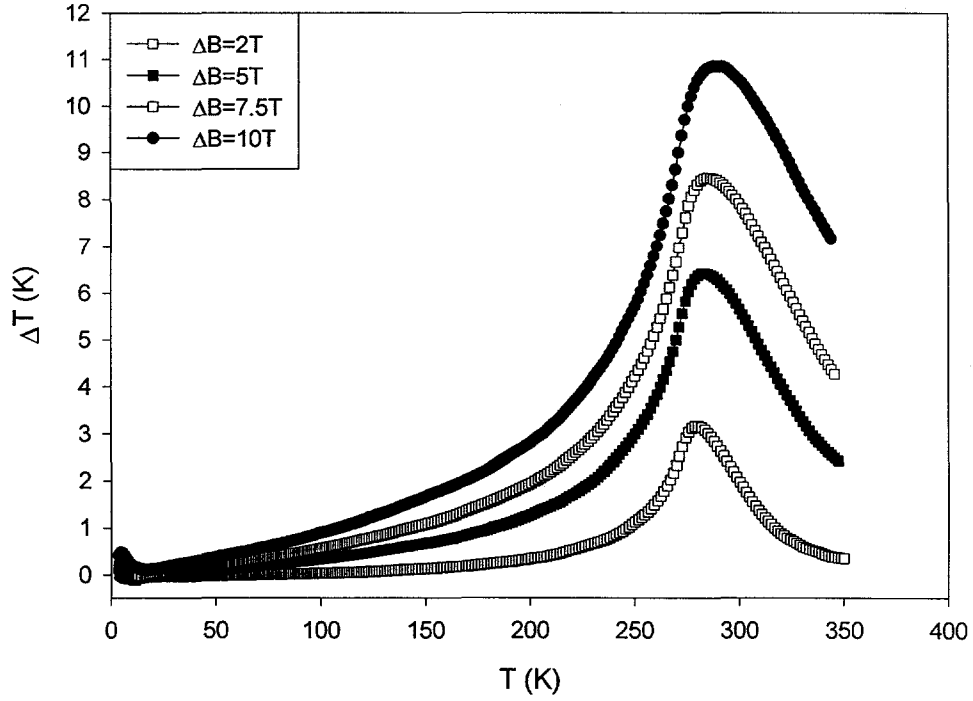

Figure 3.30 Temperature rises for $Gd_4(Bi_{0.25}Sb_{0.75})_3$ for various magnetic field changes

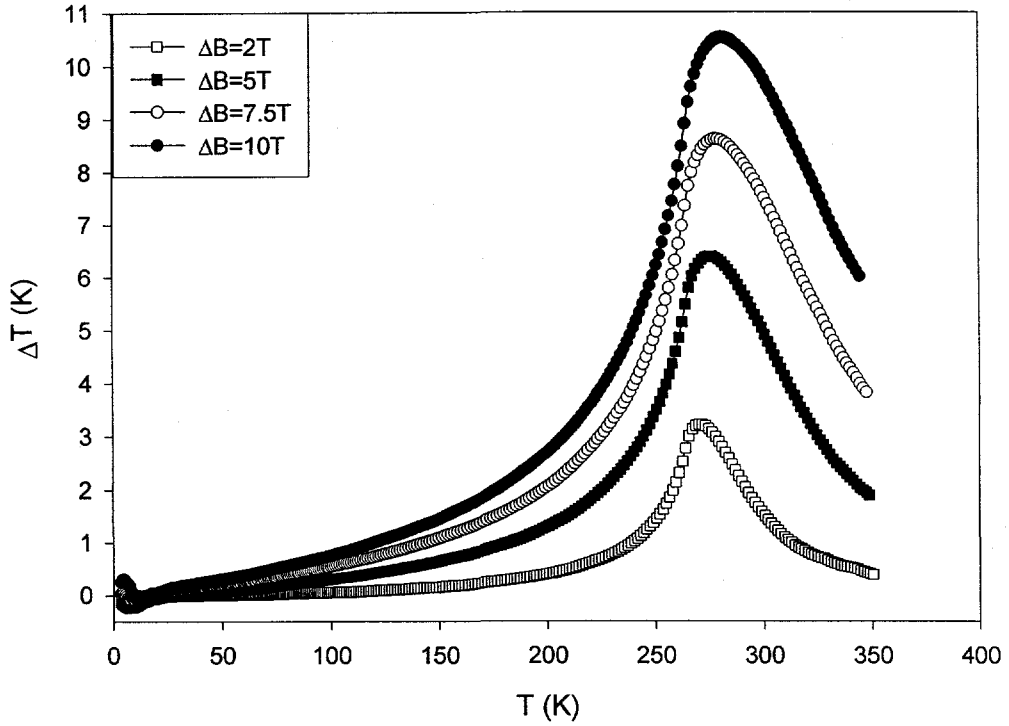

Figure 3.31 Temperature rises for Gd_4Sb_3 for various magnetic field changes

affected by the magnetic field, as predicted by a model of Tishin *et al* [19]. These temperatures are the intersection points of the zero field heat capacity curve with each of the non-zero field heat capacity curves. For ferromagnets these points should be higher than the zero field heat capacity maximum. For a second order magnetic transition the high temperature tail of the heat capacity is not a vertical line. Therefore, the intersection points made with a non-zero field heat capacity curve are not the same. Instead they increase with increasing field strength. Table 3.4 lists the temperatures of MCE peaks calculated from heat capacity data and those obtained from the magnetization measurement (i.e. the $-\Delta S_M$ data).

The temperatures of MCE maxima as determined from heat capacity data are quite close to those from $-\Delta S_M$ data, but they are consistently higher than the Curie

Table 3.4 MCE peak temperatures

Sample $Gd_4(Bi_xSb_{1-x})_3$	ΔB=B-0 (T)	MCE peak temperature (K)		Curie temperature (K)
		From C_p	From $-\Delta S_M$	
x = 0	0 [a]	268	268	
	2	270	270	
	5	274	274	266
	7.5	276	276	
	10	278	278	
x = 0.25	0	278	278	
	2	279	279	
	5	283	282	274
	7.5	283	283	
	10	285	285	
x = 0.5	0	291	291	
	2	292	292	
	5	296	296	288
	7.5	297	297	
	10	298	299	
x = 0.75	0	310	310	
	2	311	311	
	5	312	312	308
	7.5	313	313	
	10	314	314	
x = 1	0	332	334	
	2	333	335	
	5	335	336	332
	7.5	336	337	
	10	337	338	

[a] These figures are obtained by linearly extrapolating other ΔB data

temperatures. After the peak temperatures were linearly extrapolated to $\Delta B=0$, they become closer to each other. However they do not agree with each other as well as in Tishin *et al*'s work [19].

The maximum MCE values of both $-\Delta S_M$ and ΔT for a field change of 10 T are plotted as a function of Bi concentration in Figure 3.32 for the alloy series. They exhibit almost linear relationship with composition except the MCE value for Gd_4Bi_3. This may be due to the presence of a second phase in the sample.

The result of $-\Delta S_M$ from magnetization measurements and those from heat capacity measurements are compared with each other in Figures 3.33 – 3.37. As magnetization is measured only up to 5T, only curves for the 0 to 2T and 0 to 5T magnetic field changes are compared here. Within the experimental accuracy the $-\Delta S_M$ values from the two different methods agree quite well.

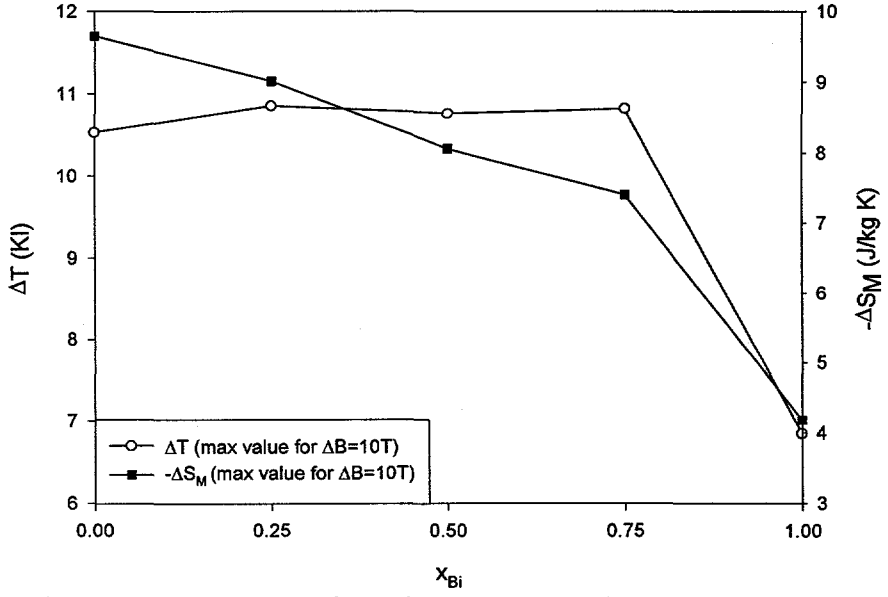

Figure 3.32 Variation of Maximum MCE and Tc with composition

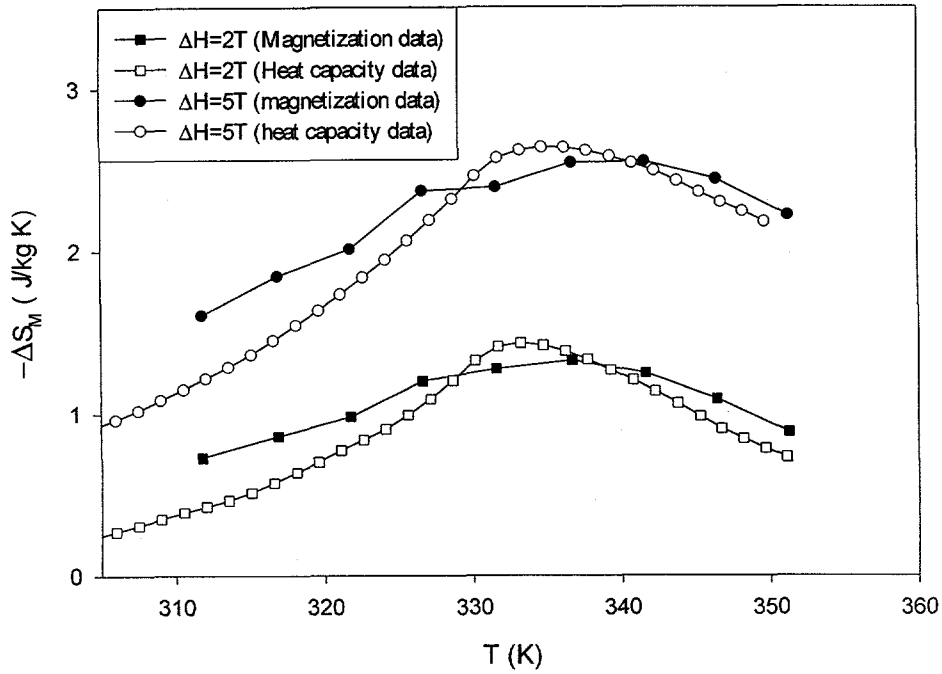

Figure 3.33 Comparison of measurements of magnetocaloric effect, $-\Delta S_M$, of Gd_4Bi_3 by different methods

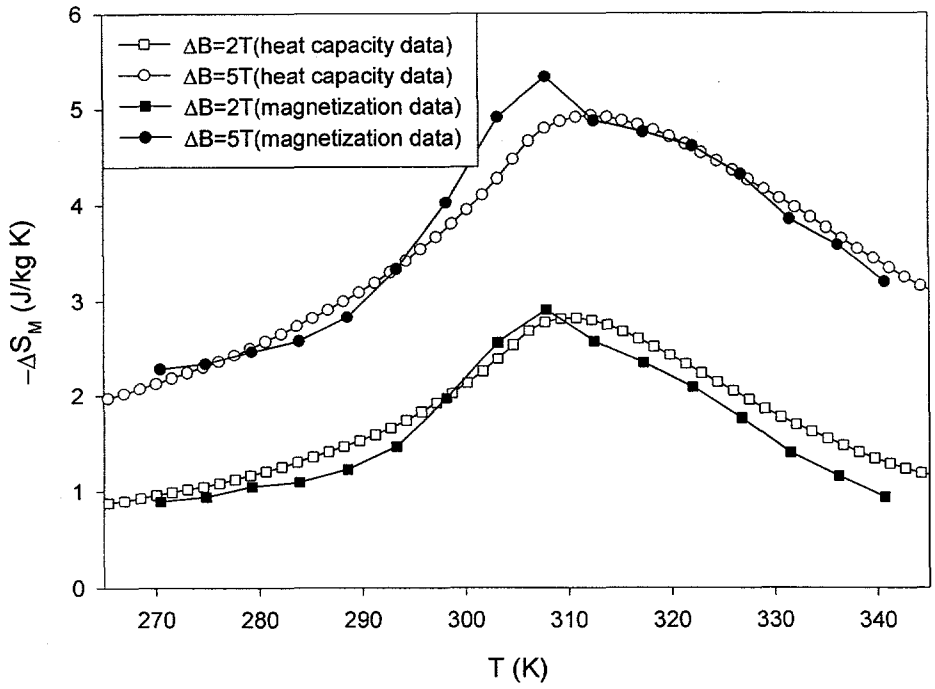

Figure 3.34 Comparison of measurements of magnetocaloric effect, $-\Delta S_M$, of $Gd_4(Bi_{0.75}Sb_{0.25})_3$ by different methods

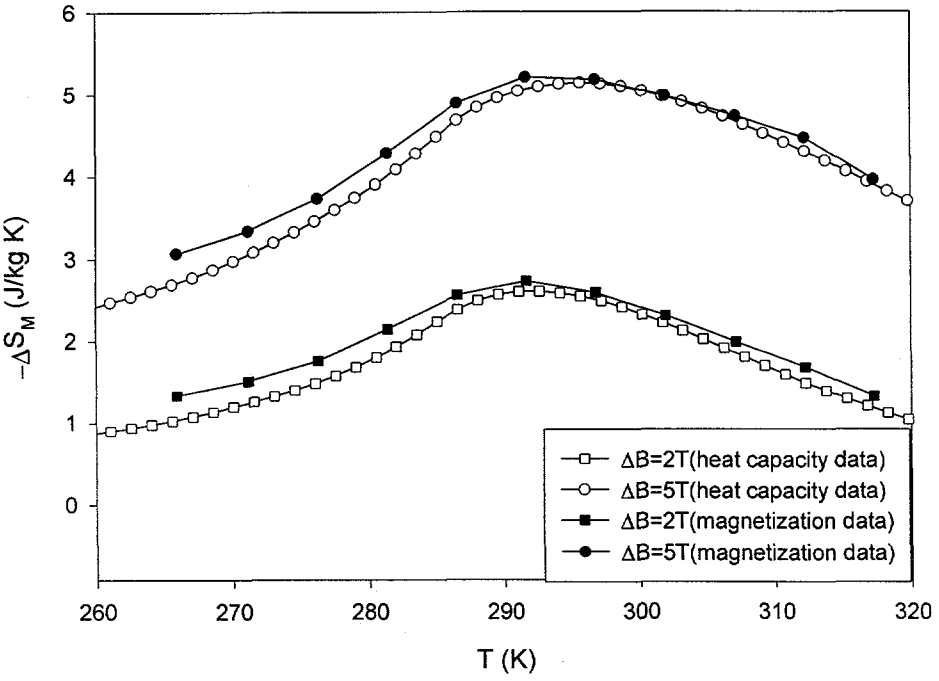

Figure 3.35 Comparison of measurements of magnetocaloric effect, $-\Delta S_M$, of $Gd_4(Bi_{0.5}Sb_{0.5})_3$ by different methods

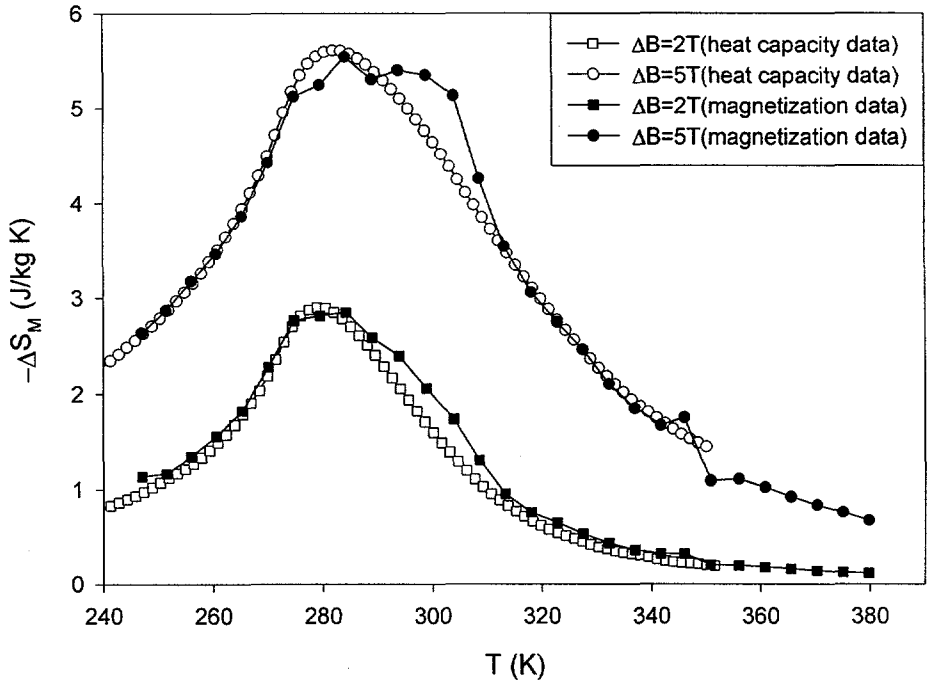

Figure 3.36 Comparison of measurements of magnetocaloric effect, $-\Delta S_M$, of $Gd_4(Bi_{0.25}Sb_{0.75})_3$ by different methods

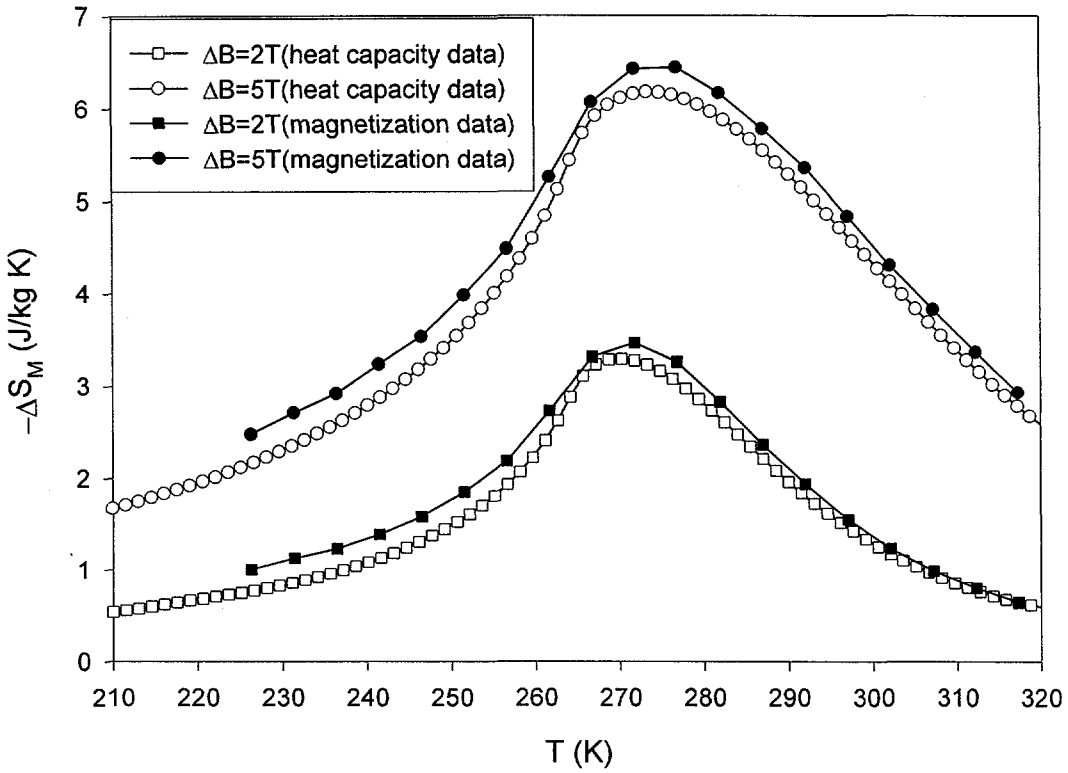

Figure 3.37 Comparison of measurements of magnetocaloric effect, $-\Delta S_M$, of Gd_4Sb_3 by different methods

The magnetocaloric effect of the $Gd_4(Bi_xSb_{1-x})_3$ alloys is moderate compared to prototype materials such as Gd. However, they have relatively good shape. The width of the peaks at half maximum can reach as high as 60 to 100K which is comparable to Gd. This feature of these materials is useful to magnetic refrigerators as it provides considerable cooling power over wide temperature range. The temperatures of the MCE peaks range from 277K to 338K. This is quite suitable for applications in near room temperature refrigeration.

4. CONCLUSIONS

Alloys from the $Gd_4(Bi_xSb_{1-x})_3$ series were prepared by melting a stoichiometric amounts of pure metals in an induction furnace. The crystal structure is of the anti-Th_3P_4 type (space group $I\bar{4}3d$) for all the compounds tested. The linear increase of the lattice parameters with Bi concentration is attributed to the larger atomic radius of Bi than that of Sb.

Magnetic measurements show that the alloys order ferromagnetically from 266K to 330K, with the ordering temperature increasing with decreasing Bi concentration. The alloys are soft ferromagnets below their Curie temperatures, and follow the Curie-Weiss law above their ordering temperatures. The paramagnetic effective magnetic moments are low compared to the theoretical value for a free Gd^{3+}, while the ordered magnetic moments are close to the theoretical value for Gd.

The alloys exhibit a moderate magnetocaloric effect (MCE) whose maxima are located between 270K and 338K and have relatively wide peaks. The peak MCE temperature decreases with decreasing Bi concentration while the peak height increases with decreasing Bi concentration.

The Curie temperatures determined from inflection points of heat capacity are in good agreement with those obtained from the magnetocaloric effect. The MCE results obtained from the two different methods (magnetization and heat capacity) agree quite well with each other for all of the alloys in the series.

REFERENCES

[1] E.Warburg, Ann.Phys. (Leipzig). 13, 141 (1881)

[2] A.H. Morrish, The Physical Principles of Magnetism, John Wiley & Sons, Inc., New York, ch. 3 (1965)

[3] D. C. Jiles, Introduction to Magnetism and Magnetic Materials, Chapman and Hall, London, New York (1991)

[4] Smart J.S., J. Appl. Phys., 81, 824 (1966)

[5] Vonsovskii S.V., Magnetism, Israel Progam Sci. Translations, Jerusalem (1974)

[6] K.A. Gschneidner, Jr. and V.K. Pecharsky, J. Appl. Phys. 85, 5365 (1999)

[7] P. Debye, Ann. Phys, 81, 1154 (1926)

[8] W.F. Giauque, J. Am. Chem. Soc., 49, 1864 (1927)

[9] C.B. Zimm, A. Jastrab, A. Steinberg, V.K. Pecharsky, K.A. Gschneidner, Jr., M.G. Osborne, and I.E. Anderson, Adv. Cryog. Eng., 43, 1759 (1998)

[10] S.K. Sinha, in K.A. Gschneidner, Jr. and L. Eyring (Eds), The Handbook on the Physics and Chemistry of Rare Earths, Vol. 1 North-Holland/Elsevier, Amsterdam, p.489 (1978)

[11] D. Gignoux and D. Schmidt, in K.A. Gschneidner, Jr. and L. Eyring (Eds), The Handbook on the Physics and Chemistry of Rare Earths, Vol. 20 North-Holland/Elsevier, Amsterdam, p.293 (1995)

[12] H. Korte, V.K. Pecharsky and K.A. Gschneidner, Jr., J. Appl. Phys. 84, 5677 (1998)

[13] C.R. Cross, J.A. DeGregoria, S.R. Jaefer, and J.W. Johnson, Adv. Cryog. Eng. 33, 767 (1988)

[14] V.K. Pecharsky and K.A. Gschneidner, Jr., Appl. Phys Lett. 70, 3299-301 (1997)

[15] F. Holtzberg, T.R. McGuire, S. Methfessel, and J.C. Suits, J. Appl. Phys., 35, 3, 1033 (1964)

[16] L.G. Akselrud, Yu. N. Grin, P. Yu. Zavalij, V.K. Pecharsky, and V.S. Fundamensky, in: XIIth Europ. Crystallogr. Meeting, Coll. Abstr., ed. B.K. Vainstein and A.M. Prokhorov, 3, 155 (1989)

[17] V.K. Pecharsky and K.A. Gschneidner, Jr., J. Appl. Phys., 86, 1, 565-75 (1999)

[18] Karl A. Gschneidner, Jr., LeRoy Eyring (Eds), Handbook on the Physics and Chemistry of Rare Earths, Vol 4: Non –metallic Compounds II, North-Holland/Elsevier, Amsterdam, p.191 (1978)

[19] A.M. Tishin, K.A. Gschneidner, Jr., and V.K. Pecharsky, Phys. Rev. B, 59, 503 (1999)

ACKNOWLEDGEMENTS

The author would like to express his gratitude toward the people who have assisted him in this project. Dr. Karl A. Gschneidner Jr. has acted as my advisor and has provided me with encouragement along the way. Dr. Vitalij K. Pecharsky's and Dr. Yevhen Levin's helpful discussions and comments have also been appreciated. Dr. Alexandra O. Pecharsky and Jack Moorman have helped by providing training on the equipment and keeping the apparati running.

This work was performed at Ames Laboratory under Contract No. W-7405-Eng-82 with the U.S. Department of Energy. The United States government has assigned the DOE Report number IS-T 1894 to this thesis.